Remote Sensing of Environment 211 (2018) 89–104

Contents lists available at ScienceDirect

Remote Sensing of Environment

journal homepage: www.elsevier.com/locate/rse

Mapping spatio-temporal dynamics of the cover and management factor (C-factor) for grasslands in Switzerland

Simon Schmidt[a,*], Christine Alewell[a], Katrin Meusburger[a,b]

[a] Environmental Geosciences, University of Basel, Bernoullistrasse 30, CH-4056 Basel, Switzerland
[b] Swiss Federal Institute for Forest, Snow and Landscape Research WSL, Zürcherstrasse 111, CH-8903 Birmensdorf, Switzerland

ARTICLE INFO

Keywords:
Monthly soil erosion modeling
Soil loss ratio SLR
R-factor
RUSLE
Vegetation dynamics
Swissimage
MODIS MOD13Q1
FCover
CCI land cover

ABSTRACT

The decrease in vegetation cover is one of the main triggering factors for soil erosion of grasslands. Within the Revised Universal Soil Loss Equation (RUSLE), a model commonly used to describe soil erosion, the vegetation cover for grassland is expressed in the cover and management factor (C-factor). The site-specific C-factor is a combination of the relative erosion susceptibility of a particular plant development stage (here expressed as soil loss ratio SLR) and the corresponding rainfall pattern (here expressed as R-factor ratio). Thus, for grasslands the fraction of green vegetation cover (FGVC) determines the SLRs. Although Switzerland is a country dominated by grassland with high percentages of mountainous regions and evidence for high erosion rates of grassland exists, soil erosion risk modeling of grasslands and especially of mountainous grasslands in Switzerland is restricted to a few studies. Here, we present a spatio-temporal approach to assess the dynamics of the C-factor for Swiss grasslands and to identify erosion prone regions and seasons simultaneously. We combine different satellite data, aerial data, and derivative products like Climate Change Initiative (CCI) Land Cover, Swissimage false-color infrared (Swissimage FCIR), PROBA-V Fraction of green Vegetation Cover (FCover300m), and MODIS Vegetation Indices 16-Day L3 Global (MOD13Q1) for the FGVC mapping of grasslands. In the spatial mapping, the FGVC is extracted from Swissimage FCIR (spat. res. 2 m) by linear spectral unmixing (LSU). The spatially derived results are then fused with the 10-day deviations of temporal FGVC derived by FCover300m. Following the original RUSLE approach, the combined FGVC are transformed to SLRs and weighted with high spatio-temporal resolved ratios of R-factors to result in spatio-temporal C-factors for Swiss grasslands. The annual average C-factor of all Swiss grasslands is 0.012. Seasonal and regional patterns (low C in winter, high C in summer, dependency on elevation) are recognizable in the spatio-temporal mapping approach. They are mainly explicable by the R-factor distribution within a year. Knowledge about the spatio-temporal dynamic of erosion triggering factors is of high interest for agronomists who can introduce areal and time specific selective erosion control measures and thereby reduce the direct costs of mitigation as well as erosion measures.

1. Introduction

Among all soil erosion risk factors in USLE-type (Universal Soil Loss Equation) and USLE based soil erosion models (e.g., RUSLE Revised Universal Soil Loss Equation), the cover and management factor namely C-factor is the one most sensitive as it follows plant growth and rainfall dynamics (Wischmeier and Smith, 1978; Nearing et al., 2005). The C-factor represents the effect of cropping and management practices on soil erosion rates by water (Renard et al., 1997). The factor can be expressed as a combination of crop and plant systems, management, and rainfall pattern (Wischmeier and Smith, 1978). Following the USLE-original approach (Wischmeier and Smith, 1978; Schwertmann et al., 1987), a site-and time-specific C-factor is derived by the ratio of soil losses (soil loss ratio SLR) of a particular crop stage period (for arable land) or plant development stage (for grassland) weighted by its corresponding fraction of rainfall erosivity (R-factor ratio; Renard et al., 1997). Thus, the rainfall erosivity is considered twice in the RUSLE: as R-factor and as a weighting factor of the C-factor (Schwertmann et al., 1987). Alternatively, SLRs are a multiplication of sub-factors (previous land use, canopy cover, surface cover, surface roughness, soil moisture; Renard et al., 1997). C-factor values are equaling 1 for bare soil of the reference plot and reach a minimum in forests (C-factor = 0.0001; Wischmeier and Smith, 1978). The C-factor is the most adjustable factor by land use management (Durán Zuazo and Rodríguez Pleguezuelo, 2008; Maetens et al., 2012; Biddoccu et al., 2014; Eshel et al., 2015; Biddoccu et al., 2016) with the highest amplitude of spatial and

* Corresponding author.
E-mail addresses: si.schmidt@unibas.ch, simon@simonschmidt.de (S. Schmidt), christine.alewell@unibas.ch (C. Alewell), katrin.meusburger@wsl.ch (K. Meusburger).

https://doi.org/10.1016/j.rse.2018.04.008
Received 21 December 2017; Received in revised form 29 March 2018; Accepted 4 April 2018

temporal variation among all the RUSLE factors (Zhang et al., 2011; Estrada-Carmona et al., 2016). Thus, the factor can easily alter by a change of policy and farming strategies (McCool et al., 1995; Panagos et al., 2015a). An alteration of the support practice factor (P) (e.g., introducing of stone walls, grass margins, contour farming, terracing) often requires higher financial investments and soil conservation subsidies (Panagos et al., 2015b, 2015c). Other important soil erosion risk factors such as rainfall erosivity (R), soil erodibility (K) and topography (LS) are mainly determined by natural conditions and are relatively more independent from anthropogenic interventions.

SLRs of grassland are preferably determined by vegetation cover fraction in contrast to arable land where plant type and/or rotation is the influencing factor (Schindler Wildhaber et al., 2012). The fractional vegetation cover is one of the most critical factors in soil erosion modeling as it describes a negatively exponential or negatively linear relationship (according to the different types of vegetation) to soil erosion (McCool et al., 1995; Puigdefábregas, 2005; Vrieling et al., 2008). A dense vegetation cover protects the soil against the raindrop splash effect (Schwertmann et al., 1987), causes a stabilization of the soil structure by plant roots (Jury and Horton, 2004; Pohl et al., 2009), enriches soils by soil organic carbon, leads to soil aggregation (Lugato et al., 2014), reduces runoff flow velocity (Bochet et al., 2006), and thus mitigates the susceptibility to soil loss (Durán Zuazo and Rodríguez Pleguezuelo, 2008; Zhou et al., 2008; Wang et al., 2009; Butt et al., 2010; Sun et al., 2013). As such, grassland cover has a high protective function for soils (Martin et al., 2010; Schindler Wildhaber et al., 2012). However, due to disturbance (García-Ruiz et al., 2015; Merz et al., 2009; Meusburger and Alewell, 2014; Sutter, 2007; Sutter and Keller, 2009; Panagos et al., 2014a), harsh climate and snow processes (Ceaglio et al., 2012; Meusburger et al., 2014), the vegetation cover can be disturbed and the consequent soil losses might be substantial. If vegetation cover is partially (66% fractional vegetation cover, Felix and Johannes, 1995) or nearly completely reduced (Frankenberg et al., 1995), erosion rates are considerably higher (4.4. t $ha^{-1} yr^{-1}$ and 20 t $ha^{-1} yr^{-1}$, respectively). Switzerland is a country dominated by grassland (Jeangros and Thomet, 2004). Nonetheless, up to now, soil erosion risk modeling is mainly restricted to arable land although evidence for high erosion rates of grasslands exists (Alewell et al., 2009; Martin et al., 2010; Meusburger et al., 2010a, 2010b, 2014; Konz et al., 2012; Meusburger and Alewell, 2014; Alewell et al., 2014).

Commonly, remote sensing approaches to determine the C-factors (Vrieling, 2006; Zhang et al., 2011; Panagos et al., 2014a) are not calculating SLRs but frequently assess the C-factor directly without weighting SLRs with the intra-annual distribution of rainfall erosivity to assess C-factors in the original sense of (R)USLE. Remote sensing methods for C-factor determination are often based on vegetation indices like the Normalized Difference Vegetation Index (NDVI). NDVIs are directly transformed to C-factors by a linear (de Jong et al., 1998) or exponential regression (van der Knijff et al., 2000) or related to field observations (Karaburun, 2010; Vatandaşlar and Yavuz, 2017). NDVI based C-factor modeling also exists for determining the C-factor for mountainous grasslands (regions of Korea, Lee and Won, 2012; China, Zhang and Li, 2015; Kyrgyzstan, Kulikov et al., 2016; Turkey, Vatandaşlar and Yavuz, 2017). However, drawbacks of that technique are its uncertainty due to the poor correlation with vegetation attributions, the soil reflectance, and the changing vitality of plants (de Jong, 1994; Vrieling, 2006; Asis and Omasa, 2007; Montandon and Small, 2008; Meusburger et al., 2010a; Grauso et al., 2015; Panagos et al., 2015b). As an alternative to NDVI-based approaches, spectral unmixing can estimate the fractional abundance of green vegetation (here called the fraction of green vegetation cover FGVC) and bare soils/bedrock simultaneously (Paringit and Nadaoka, 2003; Guerschman et al., 2009) which are related to C-factors after including rainfall erosivity (Yang, 2014). Spectral unmixing techniques (e.g., linear spectral unmixing LSU) are used in many erosion studies to determine C-factors over the last years (Hill et al., 1995; Ma et al., 2003; Lu et al., 2004; de Asis and Omasa, 2007; de Asis et al., 2008; de Jong and Epema, 2010; Meusburger et al., 2010a, 2010b). An advantage of spectral unmixing compared to traditional hard classification methods is the decomposition of mixed pixels in its corresponding component fractions rather than assigning them to a unique single class (Foody, 2006). Under consideration of the NDVI-related disadvantages, de Asis and Omasa (2007), de Asis et al. (2008) and Yang (2014) perform a comparative analysis of C-factors, derived from NDVI- and LSU-approaches, which result in better results for LSU. A relationship between C-factor and canopy cover fraction can be observed in various studies. Zhang et al. (2003) and Gao et al. (2012) determine an exponential decrease of the C-factor with an increase in canopy cover of grasslands. Wischmeier and Smith (1978) also observed a negatively exponential relationship of decreasing C-factors with increasing coverage in their empirical experiments on the USLE plots.

The (R)USLE factors C and R are highly dynamic with a clear annual cycle (Wischmeier and Smith, 1978; Renard and Freimund, 1994; Vrieling, 2006; Vrieling et al., 2014; Möller et al., 2017) in contrast to the rather constant RUSLE-factors K and LS (Panagos et al., 2012; Alexandridis et al., 2015). The status of grasslands is diversified within a year owing to the natural growth cycle, periodical cutting of hay, or pasture farming (Wiegand et al., 2008). Despite, this spatio-temporal variability of the C-factor for grasslands, it is often parameterized without accounting for the spatial variability within a land cover unit (Ozcan et al., 2008; Bosco et al., 2009; Efthimiou, 2016; Mancino et al., 2016) nor for the temporal variations (Wang et al., 2002). Hawkins (1985) stated already that “the complications of time and spatial variations in site properties are usually not considered” by applying the USLE. Alexandridis et al. (2015) conclude that a dynamic approach focusing on C-factors for the four seasons or 12 months of a year might help to reduce errors in the annual soil loss compared to a single annual C-factor. Vrieling et al. (2008, 2014) follow a multi-temporal and spatial approach to assess the riskiest erosion periods of the year for Brazil and Africa. López-Vicente et al. (2008) capture erosive periods among a year for a study area in the mountains of the Central Spanish Pyrenees by a dynamic approach on a monthly scale. Such time-dependent assessments of soil loss are relevant to support policy makers and farmers to protect the soil more targeted like it was done by López-Vicente et al. (2008). Panagos et al. (2012, 2016) and Karydas and Panagos (2016, 2017) propose a monthly time-step to be appropriate for soil erosion modeling. The same resolution was already proposed by Wischmeier and Smith (1965). Grazhdani and Shumka (2007) modeled the soil erosion rate for Albania on a monthly scale. A combination of both spatially and temporally varying R- and C-factors lead to a more dynamic soil erosion risk assessment and simultaneously allows the identification of susceptible seasons and regions (Panagos et al., 2014a; Ballabio et al., 2017; Möller et al., 2017). As it is shown in Meusburger et al. (2012), Schmidt et al. (2016) and Ballabio et al. (2017), the R-factor of Switzerland also has a high intra-annual variability with clear regional patterns.

So far, most of the existing national C-Factor maps either do not include grassland areas (Friedli, 2006; Alexandridis et al., 2015), do not consider the temporal variations of vegetation cover and management (Friedli, 2006; Bosco et al., 2009; Panagos et al., 2015b), nor taking rainfall erosivity for C-factor calculation into account. An assessment following the original approach by Wischmeier and Smith (1978) to derive C-factor maps with a high spatio-temporal resolution based on SLRs and spatio-temporal R-factor ratios does not yet exist on a national scale. We aim to (i) determine the fractional vegetation cover with a linear spectral unmixing of orthophotos (2 m spatial resolution), and (ii) quantify the temporal change of vegetation fraction (10 days temporal resolution) to (iii) assess the spatial and temporal patterns of the C-factor based on SLRs and high-spatio-temporal R-factor ratios.

Table 1
Datasets used for C-factor modeling of Swiss grasslands.

Dataset	Derived information	Resolution	Source
Swissimage FCIR	Spatial distribution of FGVC[a]	0.25 m spatial resolution, spectral bands NIR, R, G	Swisstopo, 2010
FCover300m	Temporal variation of FGVC[a]	10-day temporal resolution (2014 to 2016)	Smets et al., 2017
MOD13Q1	DOY[b] with maximum NDVI	16-day temporal resolution (2005 to 2015)	Didan et al., 2015
Swiss National Grassland Map	Extent of Swiss grasslands of 2015	300 m spatial resolution, improved with swissTLM3D and vector25	Schmidt et al., submitted
CCI Land Cover	Dynamic long-term snow occurrence	500 m spatial resolution, annual resolution (1992 to 2015)	Arino and Ramoino, 2017
SwissAlti3D	Digital elevation model	2 m spatial resolution	Swisstopo, 2017a
Rainfall erosivity	Rainfall erosivity of Swiss grasslands	100 m spatial resolution, based on 87 rainfall stations	Schmidt et al., 2016

[a] FGVC Fraction of Green Vegetation Cover.
[b] DOY Day of the Year.

2. Material and methods

2.1. Swiss grassland areas

Switzerland is a country with a high heterogeneity of climatic, topographic and edaphic conditions. Hills and mountains cover more than one-third of the state. The Swiss elevation ranges can be clustered in elevation zones (in m a.s.l. modified after Ellenberg et al., 2010: Colline zone < 800; Montane > 800–1800; Subalpine > 1800–2300; Alpine > 2300–2700; Subnival > 2700–3100; Nival > 3100), which are typical for the plant development in the Swiss Alps. Owed to these natural conditions, permanent grassland is the predominant land use in about 28% of the territory of Switzerland with a share of 72% of the total agricultural area (Bötsch, 2004; Jeangros and Thomet, 2004; Schmidt et al., submitted). Grassland is the prevailing land use type at elevations above 1500 m a.s.l. (Hotz and Weibel, 2005). Almost half (46%) of the grassland area is therefore designated as alpine grassland (Hotz and Weibel, 2005). Alpine soils have been managed by humans for about 500 years already, but an intensification of the usage and management of grasslands can be observed since the last 50 years (Jeangros and Thomet, 2004; Bätzing, 2015; Alewell et al., 2008). Changes in grassland cover are expected due to land use and climate change.

2.2. Datasets for C-factor mapping

We subdivided the datasets of the C-factor mapping approach into data for the spatial and for the temporal assessment. In the spatial modeling approach, we used a high spatial resolution false-color infrared orthophoto (0.25 to 0.50 m; G R NIR) mosaicked of a set of 3432 tiles. This orthophoto mosaic called Swissimage FCIR (Swisstopo, 2010) is recorded with a Leica ADS80 airborne digital sensor, containing the channels green (533–587 nm), red (604–664 nm) and near-infrared (833–920 nm). The production process of Swissimage FCIR is based on an along-track scanning from east to west that generates stripes of aerial photos during each flight. The scheduling of the flights of the used version of Swissimage FCIR was in the years 2012, 2013, 2014 and 2015 between the months March and September. In the preprocessing step, the aerial photos have undergone a georeferencing, orthorectification, mosaicking, and clipping to tiles of 4375 m × 3000 m by Swisstopo. We reduced the file size (original file size 1.17 Gigabytes per tile) and the spatial resolution by resampling to 2 m for a more straightforward data handling.

The temporal variations of grassland cover in Switzerland are derived from time series of 10-day fractions of the green vegetation cover (FCover300m, spatial resolution 300 m; Smets et al., 2017) as a product from PROBA-V. The FGVC is expressed in percentages from 0% (no vegetation cover) to 100% (full vegetation cover). PROBA-V is a satellite with an assembled vegetation (V) instrument to image the global land surface vegetation regularly (Blair, 2013).

A long-term recording sequence (2005–2015) of 16-day vegetation indices (MOD13Q1, spatial resolution 250 m; Didan et al., 2015) of the Moderate Resolution Imaging Spectroradiometer (MODIS) is used as supplementary data. Based on MOD13Q1, we determine the day of the year (DOY) with the highest NDVI values to be used as an indicator date for a maximum in plant growth (Leilei et al., 2014). This information is relevant for normalizing different recording periods of the Swissimage to the date of the peak growing period. A data accuracy modification was applied for MOD13Q1. Not processed or filled data, marginal data, and cloudy grid cells were substituted either by the preceding or succeeding good data or snow/ice data. With this routine, unreliable pixels were adjusted by the temporally closest reliable values.

We used the Swiss National Grassland Map of the year 2015 (Schmidt et al., submitted) for clipping the previously mentioned datasets to the grassland extent. Further, the dynamics of the long-term snow occurrence in Switzerland (Fig. S1) are derived from the Climate Change Initiate (CCI) Land Cover provided by the European Space Agency (ESA) (Arino and Ramoino, 2017). Elevation zones are extracted from the Swiss digital elevation model (SwissAlti3D, Swisstopo, 2017a). An overview of all used datasets is provided in Table 1. Data processing was done in ENVI 5.3., ESRI ArcGIS 10.3.1., and GDAL 2.1.3.

2.3. Concept of C-factor mapping for Swiss grasslands

Firstly, we derived the spatial pattern of Fraction of Green Vegetation Cover ($FGVC_{spatial}$) by LSU from the high spatial resolution Swissimage FCIR (Section 2.3.1). Secondly, we used FCover300m to estimate the temporal changes in the FGVC ($FGVC_{temporal}$; Section 2.3.2). Both approaches, the high spatial and the high temporal one are combined (Chen et al., 2015; Zhang and Li, 2015) via a normalizing procedure to result in a set of monthly FGVC maps for Switzerland (Section 2.3.3). This procedure involves the normalization of the orthophoto mosaic Swissimage FCIR with the temporal variations in vegetation cover of FCover300m to a given base date. The normalized high spatial and temporal $FGVC_{spatio\text{-}temp}$ maps of Swiss grasslands were then converted to SLR maps. The relationship of SLR and the fraction of vegetation cover (FVC) is based on measured data in alpine grasslands by Martin et al. (2010) and Schindler Wildhaber et al. (2012). SLRs were derived from the measured sediment yield for the given FVC classes proportional to an uncovered soil surface (SLR 100%; Schwertmann et al., 1987). SLR and FVC describe an exponential relationship (Eq. (1), Fig. 1). The SLRs are multiplied by the corresponding proportion of rainfall erosivity (R_{ratio}) to result in the C-factor according to the original approach by Wischmeier and Smith (1978) and Schwertmann et al. (1987). Monthly R_{ratio} for Swiss grasslands with a spatial resolution of 100 m can be obtained from Schmidt et al. (2016). The processing workflow and manipulation of data is visualized in Fig. 2.

$$SLR = e^{-0.048 * FVC} \quad \text{and} \quad FVC \approx FGVC \tag{1}$$

2.3.1. Spatial modeling of fraction of green vegetation cover ($FGVC_{spatial}$) by linear spectral unmixing

Spectral unmixing assumes that the spectrum measured by a sensor

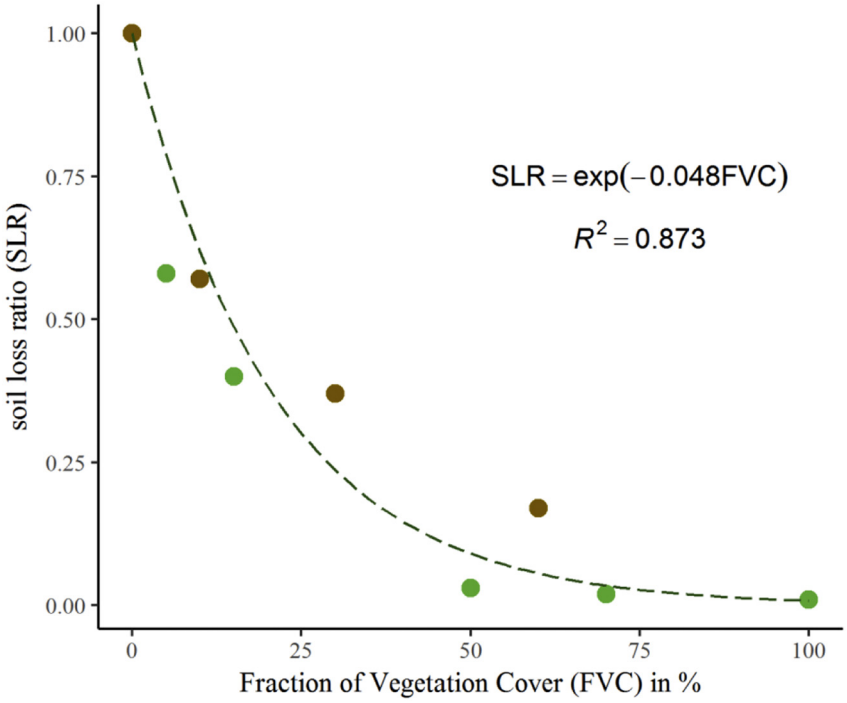

Fig. 1. Negative exponential relationship of the fraction of vegetation cover (FVC) and the soil loss ratio (SLR). The relationship of FVC and SLR results from rainfall simulations by Martin et al. (2010) (brown dots) and Schindler Wildhaber et al. (2012) (green dots). (For interpretation of the references to color in this figure legend, the reader is referred to the web version of this article.)

and represented as a mixed pixel is a combination of the spectra of components within the instantaneous field of view. As such, the reflectance of a mixed pixel is a mixture of distinct spectra (Roberts et al., 1993; Gilabert, 2000; Heidari Mozaffar et al., 2008). In spectral unmixing techniques, the mixed pixel is decomposed into a collection of endmembers and a set of fractional abundances according to the endmembers (Keshava and Mustard, 2002). The image endmembers, also called pure pixels, are at the vertices of the image simplex in an n-dimensional space (Smith et al., 1985). Pixels defined as endmembers are relatively unmixed with other endmember signals (Rogge et al., 2007). Among the spectral mixture methods, the LSU is by far the most common type (de Asis and Omasa, 2007). LSU assumes that the incoming radiation only interacts with a single component of surface and is represented in a mixed pixel without multiple scattering between different components (van der Meer, 2010). Although this is a crucial assumption, the effects of intimate association between the components have been found to be relatively minor (Kerdiles and Grondona, 1995). LSU is expressed as the spectral reflectance (R_i) of the mixed pixel in band i as followed (Smith et al., 1990; Hill et al., 1995; de Asis et al., 2008):

$$\mathbf{R_i} = \sum_{\mathbf{j=i}}^{\mathbf{n}} \mathbf{f_i r_{ij}} + \varepsilon_\mathbf{i} \text{ and } \sum_{\mathbf{j=i}}^{\mathbf{n}} \mathbf{f_i} = 1 \quad (2)$$

where j is the number of endmembers, f_j the fraction of the pixel area covered by the endmember j, r_{ij} itself is the reflectance of the endmember j in band i and ε_i the residual error in band i. In the present case, the sum of all fractions (f_j) is constrained to a value of 1 (100%; Heinz and Chein-I-Chang, 2001). A root-mean-square-error (RMSE) of the residuals for each pixel indicates the error between the measured and the modeled spectra whereas M is the total number of bands (Roberts et al., 1999; Dennison and Roberts, 2003; Bachmann, 2007):

$$\mathbf{RMSE} = \sqrt{\frac{\sum_{\mathbf{j=i}}^{\mathbf{M}} (\varepsilon_\mathbf{i})2}{\mathbf{M}}} = \sqrt{\frac{\sum_{\mathbf{j=i}}^{\mathbf{M}} (\mathbf{b_i} - \mathbf{b_i^*})2}{\mathbf{M}}} \quad (3)$$

b_i is the measured and b_i^* is the modeled signal of all the bands M. A small RMSE indicates that endmembers are appropriately selected, and its number is sufficient (Mather and Koch, 2011). LSU of QuickBird data was already applied with reasonable results for deriving vegetation parameters for an alpine grassland catchment in Switzerland (R^2 = 0.85 in relation to ground truth measurements; Meusburger et al., 2010a). However, QuickBird data is too cost intensive and heterogeneous for a national assessment and therefore rather applicable for catchment studies like it was done by Meusburger et al. (2010a, 2010b). Guerschman et al. (2009) use the hyperspectral EO-1 Hyperion in combination with MODIS data to result in a higher variety of endmembers with a spatial resolution of 1000 m. However, that spatial resolution of fractional cover is relatively coarse to explain the spatial patterns of the FGVC, SLRs and C-factors.

In the present study, orthophotos (Swissimage FCIR) with a national coverage and resampled resolution of 2 m (resampled from 0.25 m to 0.5 m) were used. The spatial assessment for deriving $FGVC_{spatial}$ (see Fig. 2) is based on all three bands of the Swissimage FCIR. ENVI 5.2 provides a Pixel Purity Index tool (PPI) to automatically identify the most spectrally pure pixels of the image, designated to be the mixing endmembers (Pal et al., 2011; RSI Research Systems, 2004). PPI works with an iterative process by counting the number of times a pixel is registered as extreme pixel for each run. Pixels that appear to be extreme most often are then endmembers (González et al., 2010). We performed 10.000 iterations with a threshold value of 2.5 and identified a maximum of 100.000 pure pixels. The application of LSU can result in n + 1 endmembers where n is the number of bands (Phillips et al., 2005). PPI based on the three bands (G, R, and NIR) of Swissimage FCIR and determined the following endmembers namely i) vegetation, ii) bedrock, bare soil, asphalt, and iii) shade. These endmembers are the typical groups of endmembers which are distributed all over the grassland areas in the country (Roberts et al., 1993; Adams et al., 1995; Theseira et al., 2003; Meusburger et al., 2010a). Although the spectrum of water is relatively pure, water was not selected as an endmember since it is occurring only locally (Adams et al., 1995).

Swissimage FCIR has undergone a Minimum Noise Fraction (MNF) rotation before the selection of purest pixel and unmixing (Green et al., 1988). The MNF rotation is a two-step principle component analysis and used to determine the inherent dimensionality of the image data, to improve the signal-to-noise ratio and reduce the processing time (Boardman and Kruse, 1994; Nascimento and Dias, 2005). MNF can improve the quality of the resulting abundance maps by a decorrelation of the bands (van der Meer and de Jong, 2000). Furthermore, since the

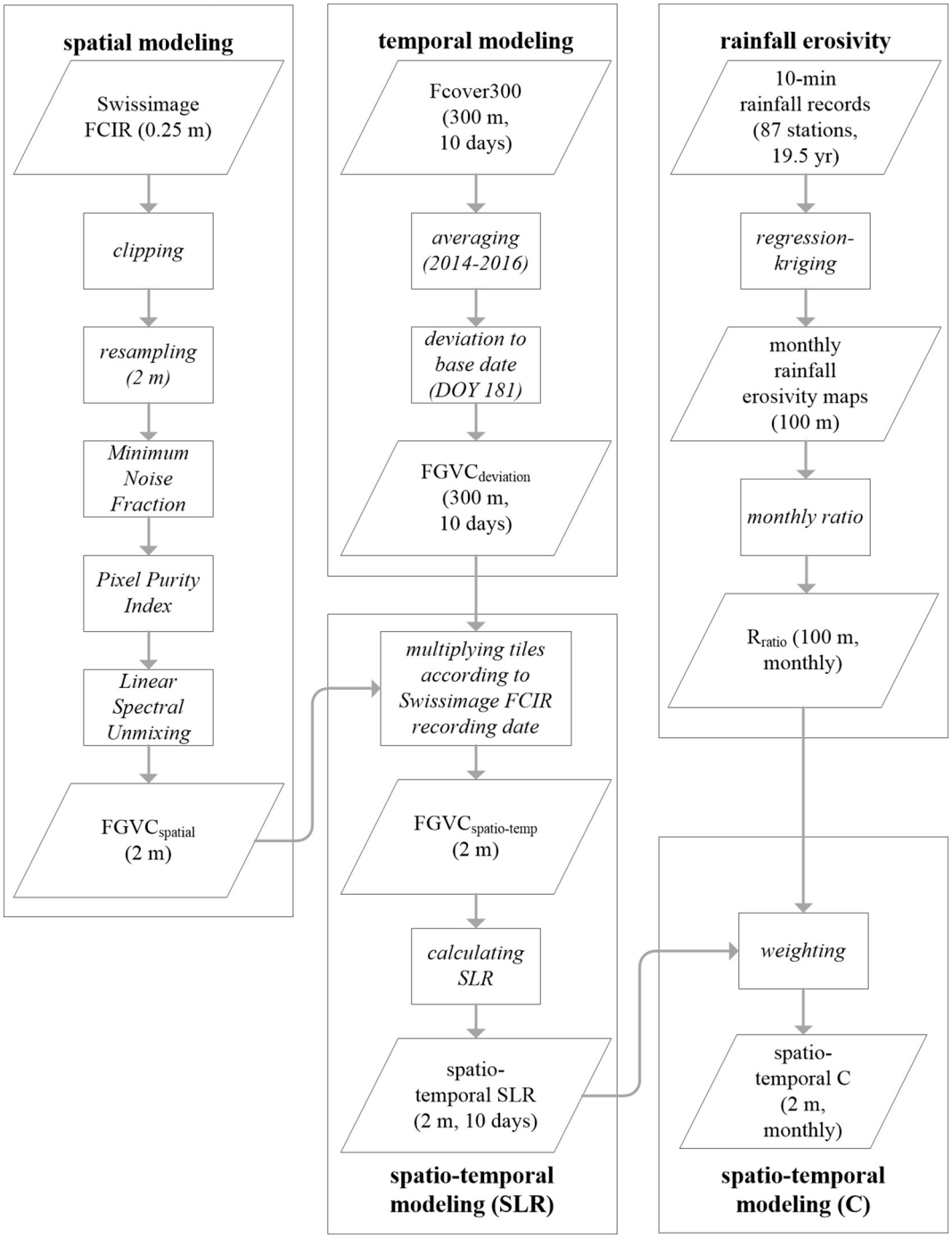

Fig. 2. Processing workflow (rectangles) of the used and derived datasets (parallelograms; detailed description of the datasets see Table 1) to result in spatio-temporal C-factors of Swiss grasslands.

spectra are neither purposed to be linked to laboratory and field reflectance spectra nor to be meant for temporal approaches, a transformation of encoded-radiances in digital numbers (DN) was not required in this study (Adams et al., 1995; van der Meer, 2002).

A well-known problem of FGVC mapping is its underestimation due to the presence of dry vegetation (Meusburger et al., 2010a, 2010b). This problem can either be addressed by long-wave spectral bands in hyperspectral sensors at the expense of spatial resolution (Guerschman et al., 2009) or by a calibration of the approach. As we aim to explain the spatio-temporal dynamics in soil erosion for Switzerland, we decided to preserve the high spatial resolution of our dataset (Swissimage FCIR) and followed the second option by using 1000 calibration points ($FGVC_{cal}$) to calibrate the $FGVC_{spatial}$ (based on the LSU) and to identify potential biases in the automated assignment of vegetation abundances. These points are randomly set for grassland areas. The $FGVC_{cal}$ is estimated user-driven for each point based on the 0.25 m resolved Swissimage FCIR and RGB. Besides that, the types of vegetation (photosynthetic and non-photosynthetic grassland, clipped grass, forest) or non-vegetation (shade, asphalt), slope degree and exposition are recorded. Although the calibration procedure assesses dry vegetation, it is not to be differentiated from bare soil in the LSU approach. Thus, the endmember of bare soil includes e.g. non-photosynthetic grassland. Thereby, the unmixed vegetation cover can be calibrated by the biases of dry vegetation. The density of optimization points is

37 km^2, corresponding to one optimization point for each 6 to 6 km on average. An acquisition of ground truth data with a representative distribution in the field is hardly feasible on a national scale.

2.3.2. Temporal mapping of fraction of green vegetation cover ($FGVC_{temporal}$ and $FGVC_{deviation}$)

Temporal variations of the fraction of green vegetation cover ($FGVC_{temporal}$) are provided within the FCover300m dataset. We averaged three files of the same date by the years 2014 to 2016 to a short-term mean fraction of green vegetation ($FGVC_{temporal}$; see Fig. 2; Smets et al., 2017). Each of the three years of FCover300m is represented by a set of 36 files (108 files in total) in a 10-day resolution from 10th of January to 31st of December. The deviation of $FGVC_{temporal}$ to a base date is determined on a per pixel scale ($FGVC_{deviation}$) to be used for normalizing the $FGVC_{spatial}$ in the following Section 2.3.3. The processing of the FCover300m data is done within the Copernicus program where FCover is derived from the leaf area index and further canopy structural variables (Smets et al., 2017). Concerning its computation, FCover300m is more robust than classical vegetation indexes like NDVI which has stronger dependencies on geometry and illumination of surface cover (Weiss et al., 2000; Fontana et al., 2008).

A series of 253 NDVI datasets from 2005 to 2015 of the MOD13Q1 (Didan et al., 2015) were used for determining this respective base date as mean peak growing season indicated by the maximum NDVI within a year (Leilei et al., 2014). Fontana et al. (2008) demonstrate that the relationship between plant growth records in alpine grasslands and NDVI is quite remarkable. Busetto et al. (2010) use a time series from 2005 to 2007 of MOD13Q1 to determine the start and the end of the growing season of larches in the alpine region. For more robust results we averaged all ten years by each specific recording date to derive a mean NDVI per recording date for Switzerland. A correction of snow cover like it was done by Busetto et al. (2010) was neglected in the study as we are only focusing on the assessment of the peak growing season and not on minimum NDVI. The maximum NDVI of all the averaged datasets was selected for each cell and the corresponding DOY assigned to the associated cell. If a cell contained a no data value, it was skipped and the averaging done over the cells of the remaining year(s).

2.3.3. Merging of spatial and temporal fraction of green vegetation cover ($FGVC_{spatio\text{-}temp}$)

As Swissimage is a mosaic of tiles recorded at heterogeneous dates, the vegetation cover can be assumed to be different between tiles according to its recording date. We used a normalizing process to make all tiles comparable. Therefore, the $FGVC_{spatial}$ are normalized to a base date. The spatial results, as well as the temporal results, are meant for being combined to spatio-temporal $FGVC_{spatio\text{-}temp}$ of grasslands (see Fig. 2). First of all, we extracted the recording dates of each along-track scanning stripe, and spatial joined the dates with the 3432 image tiles. In cases of multiple recording dates, we used the mode to extract the most common date. Tiles with same recording dates were aggregated to a multiple tile mask (Fig. S2) and later used to clip the $FGVC_{spatial}$ according to their recording dates.

Each $FGVC_{spatial}$ tileset of a specific DOY i can be normalized to that base date by weighting it with the the relative change of the $FGVC_{deviation}$ to the same base date as expressed in Eq. (4):

$$FGVC_{norm\ i} = (FGVC_{spatial\ i} * FGVC_{deviation\ i}) + FGVC_{spatial\ i} \quad (4)$$

Thus, tiles recorded early in the season where the plant growth can be assumed to be low are weighed by a greater $FGVC_{deviation}$ factor compared to an image tile recorded close to the base date.

All $FGVC_{norm}$ are merged to a new raster which represents a national map of FGVC at the defined base date. The normalized composite raster of the base date can then be recalculated to other dates.

2.4. Spatio-temporal mapping of grassland C-factors by considering soil loss ratios (SLRs) and rainfall erosivity (R-factor)

Originating from the $FGVC_{spatio\text{-}temp}$, the SLR can be calculated with the relationship proposed in Eq. (1). SLRs express the ratio of soil loss of an area with a certain plant development relative to an uncovered surface (Renard et al., 1997). The SLRs are weighted with the ratio of the total annual rainfall erosivity (R_{ratio}) of the same period to result in the C-factor. The R_{ratio} can be derived from monthly R-factor maps which exist with a high spatial resolution (100 m) for Switzerland (Schmidt et al., 2016). Monthly rainfall erosivity maps (100 m spatial resolution) for Switzerland are generated by regression-kriging of 10-min rainfall records at 87 automated gauging stations (19.5 yrs. measuring sequences) and with the use of up to five spatial covariates. The 12 maps have a mean R^2 of 0.51 and a mean RMSE of 93.27 MJ mm ha^{-1} h^{-1} month^{-1} with highest uncertainties in winter due to generally low rainfall erosivity. The authors have discussed the variability of monthly R-factors for Switzerland in detail. R_{ratio} can be assessed by calculating the monthly fraction of R-factor of the sum of all 12 maps. For the present purpose of Swiss grasslands, the monthly national maps of the R-factor are clipped to the extent of the improved Swiss National Grassland Map (Schmidt et al., submitted). The R_{ratio} maps are multiplied with the SLR maps for grassland to result in monthly C-factor maps with a high spatial resolution. For each month we averaged the three corresponding $FGVC_{spatio\text{-}temp}$ maps to monthly FGVC maps to comply with the temporal resolution of the R-factor maps.

3. Results and discussion

3.1. Spatial pattern of the fraction of green vegetation cover of Swiss grasslands

The optimized LSU of the Swissimage FCIR enables the differentiation of the $FGVC_{spatial}$ as well as the fractions for bare soil and bedrock. Spatial patterns of $FGVC_{spatial}$ are visualized on a national scale as well on a local level (Fig. 3). Such an analysis of the degree of fractional vegetation cover is of high relevance when categorizing land use for potential hot spots of erosion since it is more likely that an erosion process starts from the uncovered or bare soil.

The dimensionality of the Swissimage FCIR stays unchanged after noise segregation by MNF. The estimated ranges of $FGVC_{spatial}$ had 0.56% outliers outside the LSU constrained range of 0 to 1 (100%), which indicates that one or more of the endmembers chosen for the analysis is probably not well-characterized or that additional endmembers might be missing (RSI Research Systems, 2004). These outliers were omitted. They predominantly consisted of constructed environments (buildings, streets) that could not be masked in the grassland areas (Schmidt et al., submitted). The RMSE of the LSU for Switzerland is 22.6%. Higher uncertainties generally occur in the valleys of the Alpine foothill (Fig. 4). One reason for the high RMSE is the incorrect separation of grassland from arable land due to the coarse resolution (300 m) of the grassland map based on CCI Land Cover.

The mean FGVC of the 1000 calibration points ($FGVC_{cal}$; 61%) identifies a systematic underestimation of the mean $FGVC_{spatial}$ (39%) by 22% which is close to the mean RMSE. The highest discrepancy between $FGVC_{cal}$ and $FGVC_{spatial}$ mainly arises by an erroneous classification of non-photosynthetic vegetation (33% deviation), shades and artifacts (42% deviation), and forested areas (46% deviation). The segregation of non-photosynthetic vegetation and bare soil is impeded due to the very similar spectral characteristics. Shaded areas and artifacts disrupt the spectral signal of vegetation cover which is visually detectable but automatically assigned with a very low degree of coverage. The pattern of discrepancy between $FGVC_{cal}$ and $FGVC_{spatial}$ show a strong dependency to slope exposition. Highest deviations up to 34% are present at northern exposed slopes. All $FGVC_{spatial}$ were

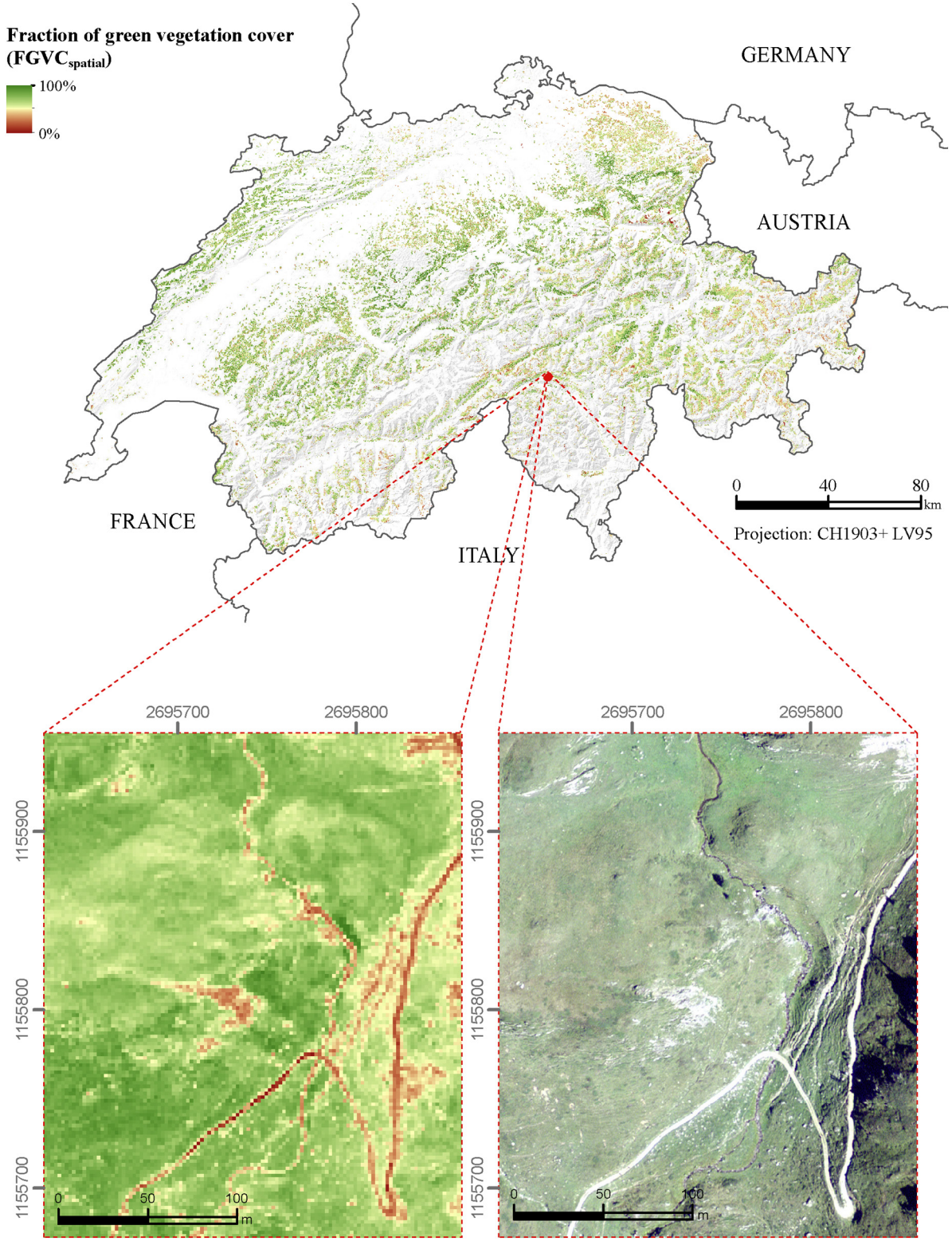

Fig. 3. Spatial patterns of the fraction of green vegetation cover (FGVC$_{spatial}$) and the orthophoto Swissimage RGB (bottom right) on different scales. The FGVC$_{spatial}$ is presented on a national and a local scale (spat. Resolution 2 m). The Swissimage RGB (spat. Resolution 0.25 m) represents the landscape on the local level. (For interpretation of the references to color in this figure legend, the reader is referred to the web version of this article.)

calibrated by adding the amount of mean underestimation to each grid cell. Subsequently, we used the calibrated FGVC$_{spatial}$ for all further calculations. The accuracy of the LSU approach could be increased with a more accurate grassland map and a higher number of spectral bands as it was already discussed in Meusburger et al. (2010a). A new orthophoto of Switzerland (Swissimage RS; Swisstopo, 2017b) with four spectral bands (NIR, R, G, B) is about to be released in 2020. Such an increase in bands could result in an additional endmember and might improve the LSU.

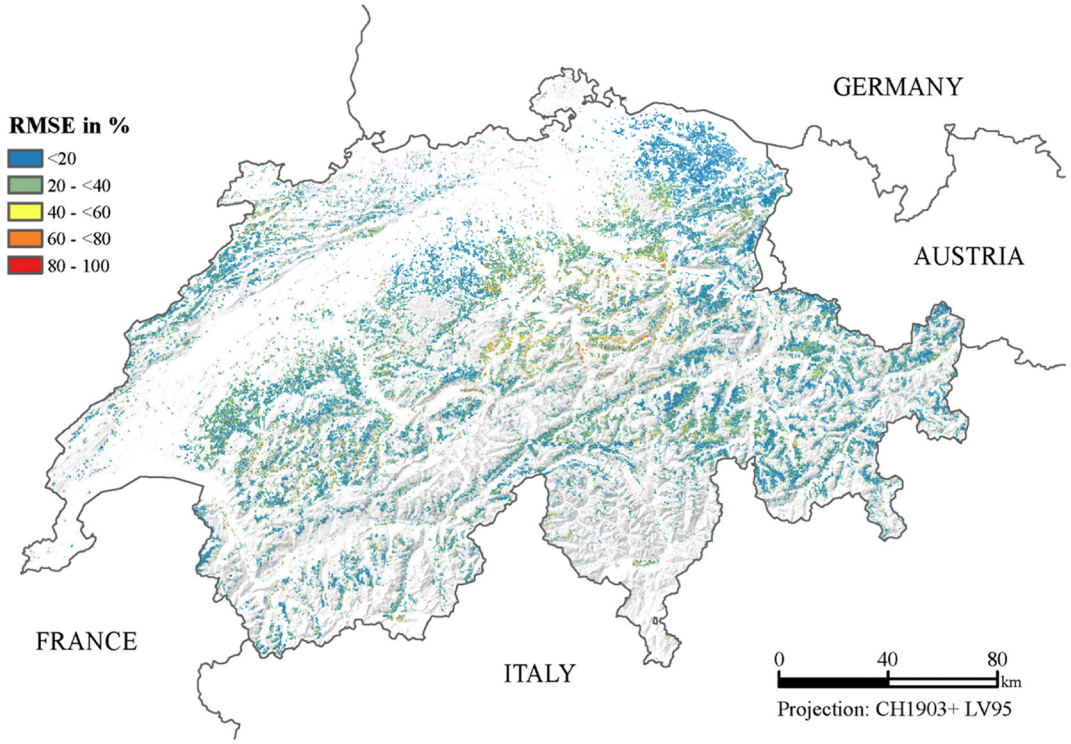

Fig. 4. RMSE of the calculated abundances based on LSU for Switzerland. (For interpretation of the references to color in this figure legend, the reader is referred to the web version of this article.)

3.2. Temporal variation in the green vegetation cover of Swiss grasslands

The annual distribution of the mean $FGVC_{temporal}$ for Swiss grasslands visualizes the seasonal dynamic of grasslands with periods of dormancy and growing (Fig. 5). Higher $FGVC_{temporal}$ lasts until the end of October (approx. DOY 304) in lower elevations (Colline and Montane zone) of northern Switzerland. According to FCover300m, an $FGVC_{temporal}$ below 40% is present for most of the Swiss grasslands from December to February. The annual distribution of the $FGVC_{temporal}$ is comprehensive and complies with the typical expectable grassland plant growth cycle (Fontana et al., 2008; Filippa et al., 2015; Inoue et al., 2015). The lack of FCover300m data mainly covers the northern latitudes of Switzerland. According to the high solar altitude in summer, missing values are relatively rare during that season. Winter records are comprised of a higher number of no data values due to snow cover (especially in the Nival zone), sun path and cloudiness (Camacho, 2016). Thus, erosion in winter continues to be a blank spot, because we can neither observe changes in FGVC below the snow cover (which will affect the SLR and C-factor) nor assess the erosivity induced by snow movement and snowmelt (which will affect the R-factor) (Ceaglio et al., 2012; Meusburger et al., 2014; Stanchi et al., 2014). We excluded no data pixels (indicating snow) from the dataset if they are presented in all the three averaged years. The FCover300m still is in demonstration mode and has only undergone a validation over Europe yet (Camacho, 2016). Therefore, uncertainty could be introduced in the absolute fraction of green vegetation cover. Nevertheless, as all the 10-day data are assessed identically, the relative deviation of the values can be deemed correctly.

Based on the MOD13Q1 data, the long-term (2005 to 2015) maximum NDVI of the most considerable proportion of pixels is DOY 177 (26th of June, Fig. S3). We used the 30th of June (DOY 181) as the base date as this date has a high temporal proximity to the maximum NDVI of our analysis. This is in agreement with Jonas et al. (2008) who proposed the 6th of July as the mean date of the maximum height of grassland cover for elevations between 1560 and 2545 m a.s.l.. According to model results by Garonna et al. (2014), the growing season in the alpine zone starts at DOY 118 and lasts until DOY 266. The $FGVC_{deviation}$ in relation to DOY 181 marks a positive trend from DOY 181 to DOY 232 which determines the peak growing season for the national grassland area (Table 2). The minimal FGVC in relation to DOY 181 is met on DOY 20 with a reduction of 58% in green vegetation cover.

3.3. Spatio-temporal patterns of the fraction of green vegetation cover of Swiss grasslands

The mean $FGVC_{spatio\text{-}temp}$ of Swiss grasslands on DOY 181 (30th of June; Fig. 6) is 60%. Grasslands next to the border of Austria (Cantons Appenzell and St. Gallen) have the lowest $FGVC_{spatio\text{-}temp}$. These Cantons (see a map of Swiss cantons in Fig. S4) are fully dominated by meadows and alpine pastures (Table 3; Federal Statistical Office Switzerland, 2017). As the management of these grasslands is very intense (grazing, fodder), the $FGVC_{spatio\text{-}temp}$ is comparatively low. Intense grazing causes a significant limitation in grass growth (Bilotta et al., 2007; Mayer et al., 2009) which results in a degradation of vegetation cover (Yong-Zhong et al., 2005). These regions have one of the highest mean livestock unit (1.7 per ha; Table 3) and mean share of grazing livestock farming (78.8%). Hence, most of the areas in the region are already mowed at the 30th of June (typical mowing period for St. Gallen is DOY 166 to DOY 196; Zwingli, 2017). The whole Switzerland experienced a land use intensification of grassland over the last decades. It is apparent by an increase in stocking rates (~50% increase of sheep numbers during 40 years) and an alteration in grazing systems (permanent shepherding replaced by uncontrolled grazing, Troxler et al., 2004).

3.4. Spatial and temporal hot-spots of C-factors on Swiss grasslands

The monthly maps (Fig. S5) are averaged to seasonal maps of C-factors for grasslands (Fig. 7). They represent the high temporal and

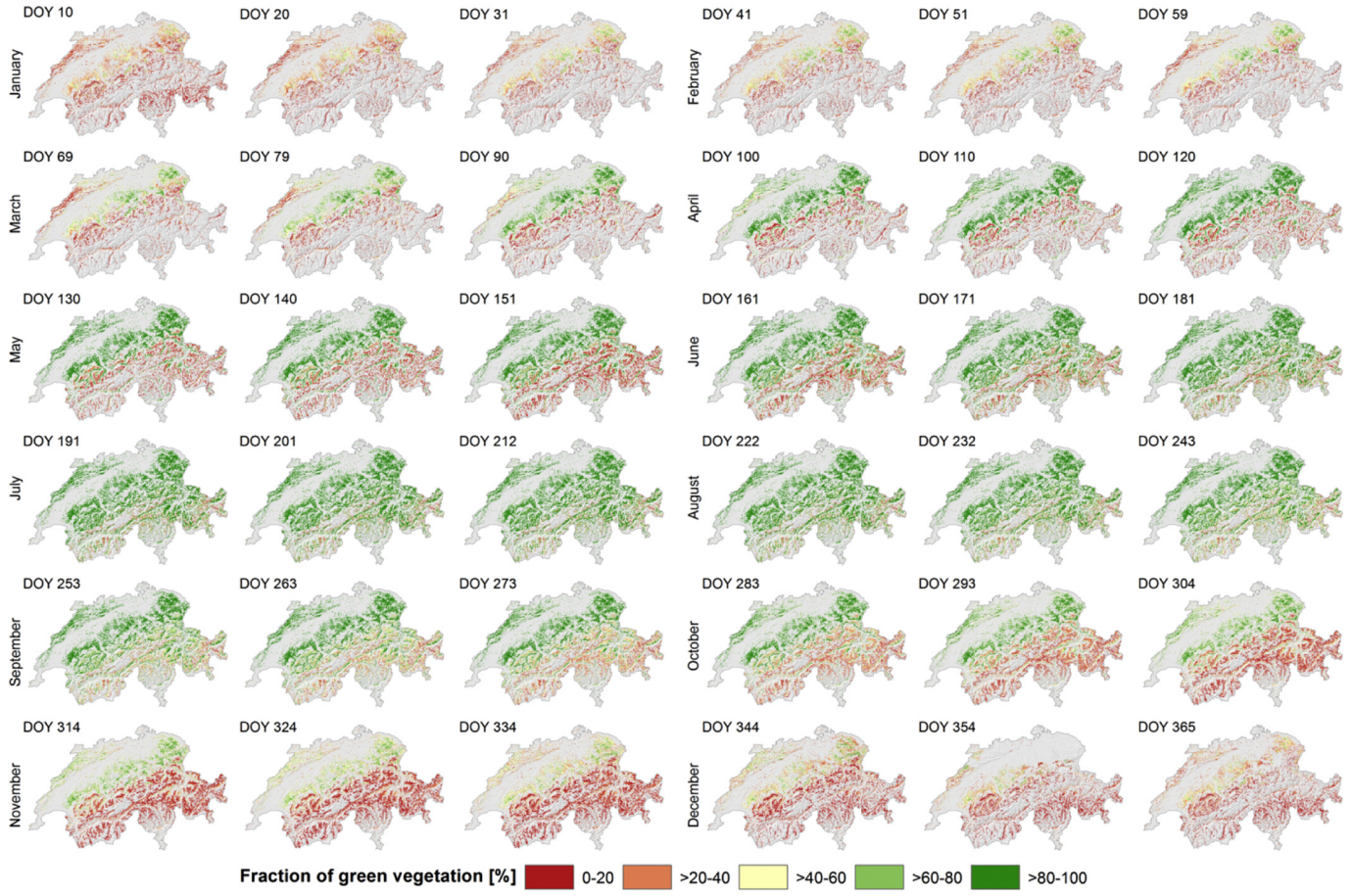

Fig. 5. Mean (2014 to 2016) $FGVC_{temporal}$ for Swiss grasslands. Mean $FGVC_{temporal}$ are derived and averaged from FCover300m from 2014 to 2016 (DOY = day of the year). (For interpretation of the references to color in this figure legend, the reader is referred to the web version of this article.)

Table 2
Mean national deviation of FGVC ($FGVC_{deviation}$) to the base date of DOY 181 (30th of June) by FCover300m.

DOY[a]	Date	$FGVC_{deviation}$ relative to DOY[a] 181 in %	DOY[a]	Date	$FGVC_{deviation}$ relative to DOY[a] 181 in %
10	Jan 10	−57	191	Jul 10	2
20	Jan 20	−58	201	Jul 20	3
31	Jan 31	−55	212	Jul 31	3
41	Feb 10	−53	222	Aug 10	3
51	Feb 20	−51	232	Aug 20	1
59	Feb 28	−50	243	Aug 31	−2
69	Mar 10	−49	253	Sep 10	−6
79	Mar 20	−44	263	Sep 20	−9
90	Mar 31	−39	273	Sep 30	−14
100	Apr 10	−31	283	Oct 10	−20
110	Apr 20	−25	293	Oct 20	−45
120	Apr 30	−24	304	Oct 31	−34
130	May 10	−22	314	Nov 10	−40
140	May 20	−20	324	Nov 20	−45
151	May 31	−17	334	Nov 30	−48
161	Jun 10	−10	344	Dec 10	−53
171	Jun 20	−5	354	Dec 20	−56
181	Jun 30	0	365	Dec 31	−56

[a] DOY Day of the Year.

spatial variability of the C-factors for grasslands throughout a year. According to the modeling results, relative high C-factors in winter can only be observed in the Jura mountain at the border to France and the western Alps. These patterns are mainly controlled by the ratio of the annual rainfall erosivity (R_{ratio}; Fig. 8). The whole alpine range experiences increased values in spring. The distribution of C-factors in summer for Swiss grasslands is relative diffuse with a spatial cluster in the north-eastern region of Switzerland (Cantons Appenzell and St. Gallen) which is a result by the low FGVC due to intense grassland land use (see Section 3.3) and the high rainfall erosivity. Absolute C-factors are decreasing in fall but with regional pattern of high C-factors at the southern and eastern Alps. The minimum C-factors within a year are covering the lowland areas of Switzerland in winter. Maximum C-factors are observable in the previously mentioned region of the Cantons Appenzell and St. Gallen (close to the border of Austria) in summer.

The mean annual C-factor for Switzerland is 0.012 (Table 4). Lowest mean C-factors of Swiss grasslands can be observed in January (0.003), highest in the summer months July (0.024) and August (0.025) (Fig. 9). The maximum C-factor in August is about 8 times higher than the minimum C-factor in January. The trend marks an abrupt increase of C-factors from April to August with a decrease in its low winter values. The natural plant growth cycle determines the annual trend of FGVC. As the C-factor is not solely related to FGVC but further a product of SLR and weighted R-factor ratios, the trend of the C-factor is influenced by the regional and temporal rainfall erosivity pattern.

The rainfall erosivity, as well as the FGVC, is controlled by elevation level (Fig. 10). The C-factors per month and elevation zone follow typical patterns. Highest C-factors can be observed in the Alpine zone. The Subalpine, Alpine and Subnival zone show more than one peak with highest C-factors. The Colline and Montane zone have only one maximum in August. The C-factors in all elevation zones are lowest in the winter months January and February. FGVC in winter is low due to the reduced plant growth. The here excluded presence of snow cover in winter results in a delay of increasing FGVC with elevation after melt-out. The typical melt-out at elevations between 1560 and 2545 m a.s.l.

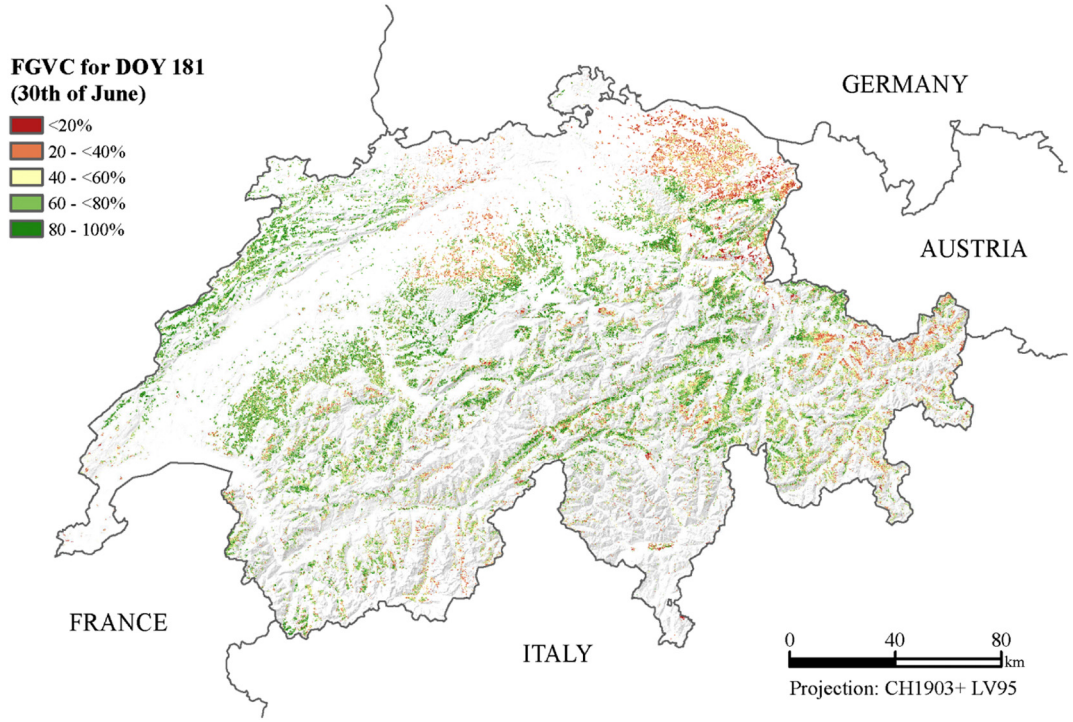

Fig. 6. Spatial pattern of the C-factor for grasslands in Switzerland for the base date DOY 181 (30th of June; spatial res. 2 m). (For interpretation of the references to color in this figure legend, the reader is referred to the web version of this article.)

is recorded by Jonas et al. (2008) and Fontana et al. (2008) at DOY 147. Large areas of Switzerland show a snow occurrence in winter (Fig. S1). Protection of grassland soils by plant cover is relatively low in winter but simultaneously affected by only very low rainfall erosivity. However, the tremendous impact of snow gliding on exposed soil surfaces during winter might be a crucial impact (Meusburger et al., 2014). Although the fraction of vegetation cover is increasing in summer for all the grasslands, the weighting with the R_{ratio} causes a high C-factor. As discussed in Schmidt et al. (2016), a significant fraction of the annual rainfall erosivity is within the time window between June and September. The predominantly glaciated Nival zone (> 3100 m a.s.l.) could not be considered due to a small proportion of grassland areas (0.6% of the zone).

Cantons in the east of Switzerland (Fig. S6) have slightly higher C-

Table 3
Averaged seasonal $FGVC_{spatio\text{-}temp}$ and agricultural intensity (Federal Statistical Office Switzerland, 2017) of the year 2016 per Swiss Canton.

Canton	Short name	$FGVC_{spatio\text{-}temp}$ (%)					Livestock unit (per hectare)	Grain farming[a] (%)	Grazing livestock farming[b] (%)
		annual	winter	spring	summer	fall			
Aargau	AG	44.5	30.6	50.2	55.0	40.6	1.2	24.1	37.2
Appenzell Ausserrhoden	AR	28.7	16.8	29.6	37.5	28.3	1.5	0.1	85.8
Appenzell Innerrhoden	AI	46.6	29.7	45.5	61.7	45.3	1.9	0	78.5
Basel-Landschaft	BL	40.6	27.0	45.1	51.7	36.7	1	15.7	46.0
Bern	BE	50.0	27.7	46.1	70.4	46.8	1.3	12.9	64.4
Fribourg	FR	51.7	32.0	54.2	68.4	50.8	1.4	16.9	55.7
Glarus	GL	48.4	20.5	34.0	72.4	40.7	1.3	0.1	95.4
Graubünden	GR	43.0	21.2	28.1	60.6	36.3	0.9	1.7	77.0
Jura	JU	58.3	35.1	61.3	77.7	56.2	1	15.1	65.0
Lucerne	LU	52.2	36.1	56.6	65.7	49.7	2.1	9.7	56.3
Neuchâtel	NE	58.2	29.3	56.5	79.9	58.7	0.9	8.3	63.4
Nidwalden	NW	47.9	26.9	44.8	69.5	43.2	1.7	0	88.3
Obwalden	OW	48.2	26.0	39.1	69.6	42.8	1.8	0	88.9
Schaffhausen	SH	50.1	32.3	55.5	65.2	42.6	0.8	33.9	14.5
Schwyz	SZ	49.4	27.6	46.0	68.5	45.8	1.4	0.4	86.5
Solothurn	SO	50.7	30.4	54.5	67.2	47.5	1.1	18	53.1
St. Gallen	SG	43.7	25.5	40.9	58.4	40.6	1.7	1.9	72.4
Thurgau	TG	30.7	21.5	33.4	37.5	29.1	1.7	17.5	38.4
Ticino	TI	46.5	24.5	29.1	63.7	40.6	0.8	4.6	40.2
Uri	UR	48.7	21.1	31.1	68.3	40.8	1.2	0	92.0
Valais	VS	45.3	22.0	30.9	61.6	38.6	0.7	2.7	40.3
Vaud	VD	49.5	25.0	45.4	71.8	47.1	0.8	28.3	24.5
Zug	ZG	55.7	32.6	60.0	73.4	54.2	1.7	5.7	70.6
Zürich	ZH	50.6	30.7	55.1	65.4	48.8	1	19.2	40.3

[a] of the total agricultural land.
[b] of total farming.

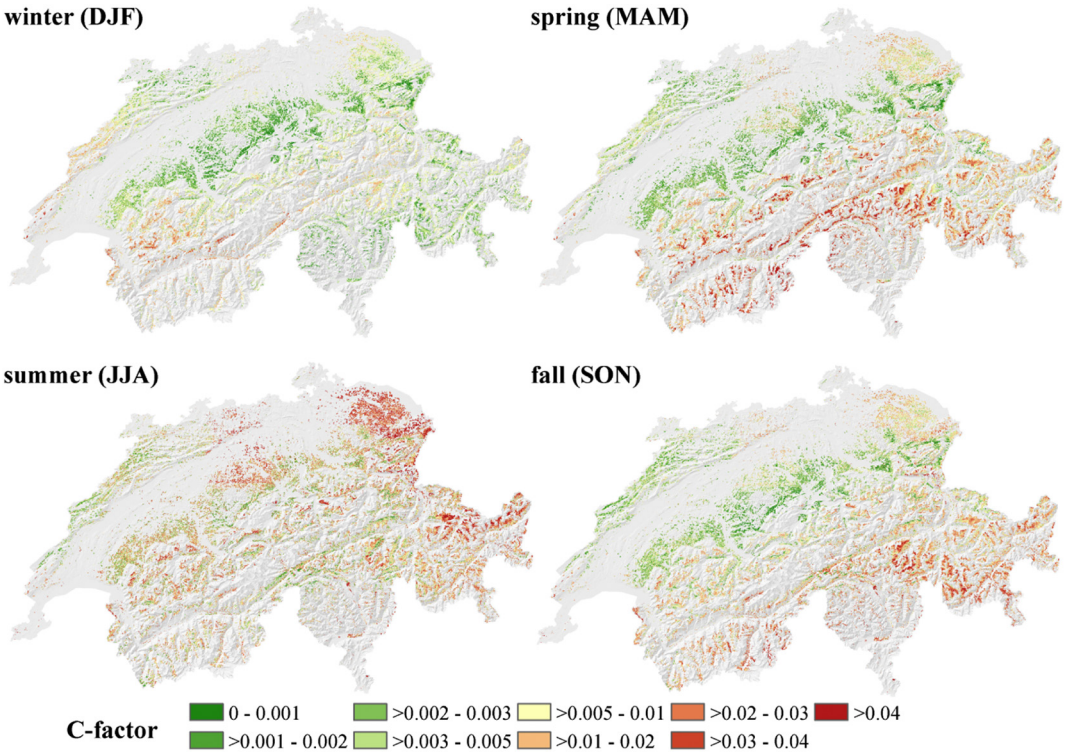

Fig. 7. Spatio-temporal variation of C-factors of Swiss grasslands per season (spar. res. 100 m). C-factors are a product of soil loss ratios and weighted rainfall erosivity ratios. The seasonal C-factors are an average of three monthly C-factor maps. (For interpretation of the references to color in this figure legend, the reader is referred to the web version of this article.)

factors in the month May to December which is also related to the differences elevation level (mean elevation of eastern cantons 1122 m a.s.l., western cantons 865 m a.s.l.) and different ratios of R-factors. The elevation patterns become also visible by comparing the northern and southern cantons (mean elevation 928 m a.s.l. and 1795 m a.s.l., respectively). The capturing of the relationship between C-factor and elevation zone meets our expectations and confirms the plausibility of the input parameters and modeling approach. Bosco et al. (2009) already observed a relationship of C-factors and elevation level based on literature values.

Kulikov et al. (2016) studied the temporal variations of C-factors of Kyrgyz mountain grasslands. They observed decreasing C-factors from April (immediately after snowmelt) to June in both of their study areas. They assess the months April and May with the highest potential soil loss owing to high C-factors with simultaneous high rainfall erosivity. A soil erosion assessment for a watershed in Brazil (de Carvalho et al., 2014) reveals highest soil loss in the rainy season where rainfall erosivity is high and the C-factor low. Another combination of dynamic R- and C-factors, done by Panagos et al. (2014b) for Crete in Greece, assesses March as a month with high rainfall erosivity and low fractional vegetation cover. Thus, it is important for C-factor assessment to consider the relative timing of peak C– and peak R-Factor.

Panagos et al. (2015b) derived C-factors for grasslands for the 28 European Union member states from FCover300m and ranges of literature values. Their results present a mean European grassland C-factor of 0.0435 which is about 3.5 times higher than the one for Switzerland. However, C-factors in Mediterranean regions, which are included in the mean European C-factor, are substantially higher than ones in Central Europe. The surrounding countries of Switzerland have mean national values between 0.0345 (Austria) to 0.0421 (Germany). Switzerland's nationwide C-factor for grasslands (0.012) is 70% lower than the mean of the four neighboring countries (0.0396). A different seasonal trend and lower values compared to Panagos et al. (2015b) and Kulikov et al. (2016) can be explained by the different methods to compute C-factors and the neglecting of the rainfall erosivity.

Extensive pasture systems might have a positive effect on a dense vegetation cover. Furthermore, rotation grazing systems or reduced stocking rates supports the development of a better-closed vegetation cover (Troxler et al., 2004). The exclusion (e.g., by fencing) of susceptible soils or spots with a reduced growth period due to a late melt-out could effectively prevent soils from being mobilized. The regeneration time of a degraded sward will take many years, and as long as then the soil surface remains uncovered, it will be fragile and highly prone to an expansion of soil degradation in the form of erosion.

The study of the dynamic soil erosion is of high importance as growing seasons in the European Alps are about to be extended under futures changing climates and shortened snow-cover periods (Defila and Clot, 2001; Studer et al., 2005; Bänninger et al., 2006; Fontana et al., 2008; Frei et al., 2017). A long-term effect of the prolonged growing season for alpine plants would be the favoring of higher and faster-growing plants with enhanced biomass production. More biomass production increases the vegetation cover and lowers the C-factor in summer (Rammig et al., 2010). Simultaneously, the warmer climate and heavy precipitation events during fall and winter will result in higher R-factors (after snowmelt; Fuhrer et al., 2006; Rajczak et al., 2013; Rajczak and Schär, 2017). Sparsely covered soils in late fall (before snow cover) and early spring are then more susceptible to erosion by water. A significant increase and intensification in the cold-season precipitation is already observable for Switzerland (Widmann and Schär, 1997; Schmidli et al., 2002; Schmidli and Frei, 2005).

4. Conclusion and outlook

We derived Swiss C-factor maps of grasslands from soil loss ratios weighted with R-factor ratios in using the most state-of-the-art remote sensing products for Switzerland (e.g., national orthophoto with an original spatial resolution of 0.25 m (Swissimage FCIR) and a 10-day time series of fractional green vegetation cover (FGVC, FCover300m)).

Fig. 8. Monthly ratio maps of the annual rainfall erosivity (R-factor) of Swiss grasslands. Monthly R-factor ratios are the fraction of R-factor related to the total annual R-factor sum. Rainfall erosivity maps of Switzerland are based on Schmidt et al. (2016). (For interpretation of the references to color in this figure legend, the reader is referred to the web version of this article.)

Table 4
Mean C-factors of Swiss grasslands per month.

Month	Mean C-factor of Swiss grasslands
January	0.003
February	0.004
March	0.005
April	0.005
May	0.018
June	0.016
July	0.024
August	0.025
September	0.015
October	0.012
November	0.013
December	0.008
Ø	0.012

The assessment enables the nationwide quantification of the C-factor of grasslands in its dynamic throughout a year. C-factors are much higher in winter than in summer due to the relation to rainfall erosivity ratio and show the expected dependency on elevation gradient. The mean annual C-factor of Swiss grasslands is 0.012 which complies with the C-factor of October. An improved spectral resolution will be available with the future Swissimage RS product which might increase the accuracy and quality of the linear spectral unmixing results. However, the present results can help to implement soil conservation strategies of an adopted land use management. The identification of regions in Switzerland and periods of the year with high C-factors in combination with the dynamic R-factors might help agronomists to introduce selective mitigation strategies for erosion control of Swiss grasslands. The mitigation potential of soil erosion particularly relies on the C-factor since the R-factor is climate driven and not directly to be altered by human interventions. The utilized grassland areas of Switzerland are of particular interest since grazing might degrade soil functions and stability and has an impact on soil cover. Grazing in alpine environments usually takes place during the most susceptible season. As sediment yield is reduced to a minimum under closed vegetation cover, priority should be on keeping the vegetation coverage of grassland high. The FGVC can be increased, and thus the C-factor lowered by avoiding grazing on highly susceptible grassland or at least by paying more attention to the choice of the grazing animal species and stocking numbers/ diversity. To capture the spread of degraded surfaces, the automated identification and classification of bare soil spots with a higher spectral resolution is envisaged for future studies. Beyond the current state of C-factors, the models can be linked to land use and climate scenarios to get an idea of future impacts of soil erosion. As we demonstrated the usefulness and applicability of the C-factor and its relation to the R-factor, this study also highlights the advantages of USLE-type modeling. Individual computation and assessment of every single factor result in a high transparency and verifiability of USLE-based erosion models. Each individual factor does not only have the advantage to be adjusted and evaluated on its own but also deliver valuable conclusions for other environmental issues.

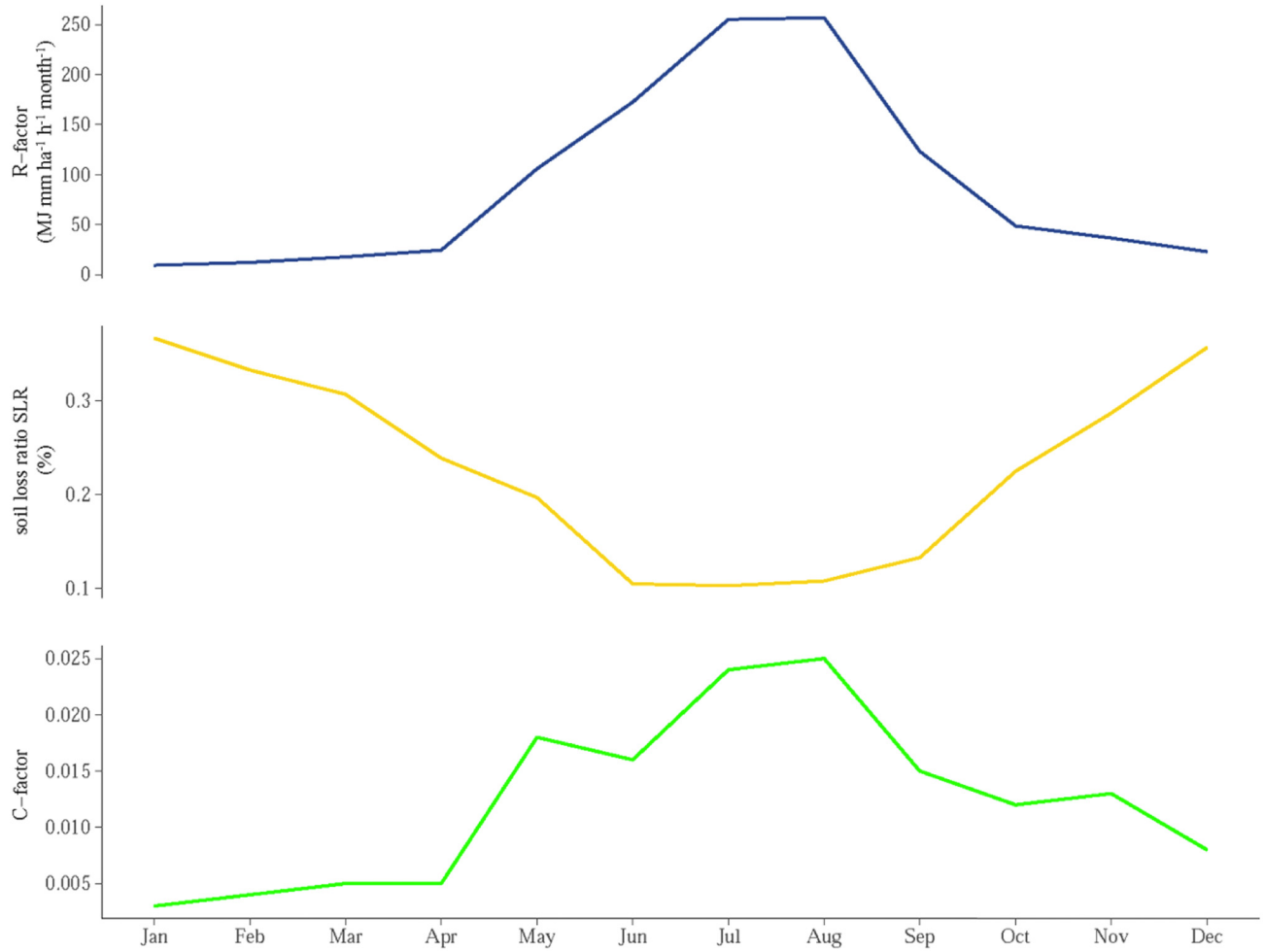

Fig. 9. Seasonal distribution of national monthly R-factors (MJ mm ha^{-1} h^{-1} $month^{-1}$), soil loss ratios (SLR; %), and C-factors of Swiss grasslands. C-factors are a product of soil loss ratios and weighted rainfall erosivity ratios. (For interpretation of the references to color in this figure legend, the reader is referred to the web version of this article.)

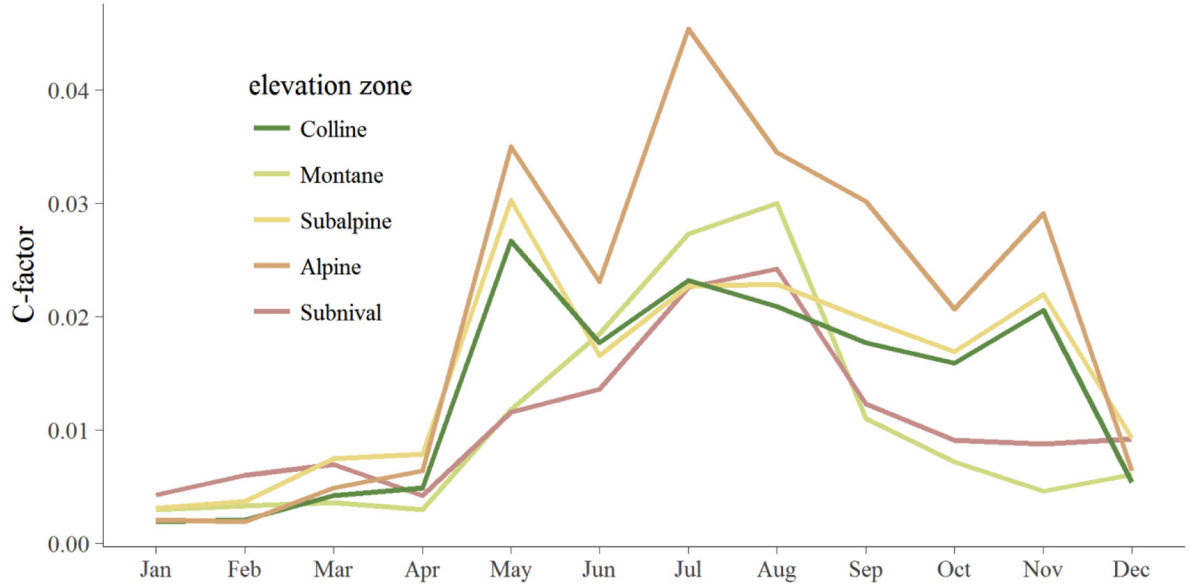

Fig. 10. Mean monthly C-factors of grasslands for different elevation zones in Switzerland. (For interpretation of the references to color in this figure legend, the reader is referred to the web version of this article.)

Acknowledgement

This work was supported by the Swiss Federal Office for the Environment (FOEN) (grant numbers N° N222-0350 and N° P182-1535). The authors would like to thank all data providers, namely Swisstopo, Copernicus Global Land Services, European Space Agency (ESA), and National Aeronautics and Space Administration (NASA) for making their data available. Furthermore, we would like to thank the anonymous reviewers for their valuable comments and suggestions to improve the quality of the paper.

Funding

This work was supported by the Swiss Federal Office for the Environment (FOEN) (grant numbers N° N222–0350 and N° P182–1535).

Declaration of interest

None.

Appendix A. Supplementary data

Supplementary data to this article can be found online at https://doi.org/10.1016/j.rse.2018.04.008.

References

Adams, J.B., Sabol, D.E., Kapos, V., Filho, R.A., Roberts, D.A., Smith, M.O., Gillespie, A.R., 1995. Classification of multispectral images based on fractions of endmembers. Application to land-cover change in the Brazilian Amazon. Remote Sens. Environ. 52, 137–154. http://dx.doi.org/10.1016/0034-4257(94)00098-8.

Alewell, C., Meusburger, K., Brodbeck, M., Bänninger, D., 2008. Methods to describe and predict soil erosion in mountain regions. Landsc. Urban Plan. 88, 46–53. http://dx.doi.org/10.1016/j.landurbplan.2008.08.007.

Alewell, C., Schaub, M., Conen, F., 2009. A method to detect soil carbon degradation during soil erosion. Biogeosciences 6, 2541–2547. http://dx.doi.org/10.5194/bg-6-2541-2009.

Alewell, C., Meusburger, K., Juretzko, G., Mabit, L., Ketterer, M.E., 2014. Suitability of 239 + 240Pu and 137Cs as tracers for soil erosion assessment in mountain grasslands. Chemosphere 103, 274–280. http://dx.doi.org/10.1016/j.chemosphere.2013.12.016.

Alexandridis, T.K., Sotiropoulou, A.M., Bilas, G., Karapetsas, N., Silleos, N.G., 2015. The effects of seasonality in estimating the C-factor of soil Erosion studies. Land Degrad. Dev. 26, 596–603. http://dx.doi.org/10.1002/ldr.2223.

Arino, O., Ramoino, F., 2017. Land Cover CCI. Product User Guide Version 2.0. Louvain-la-Neuve.

de Asis, A.M., Omasa, K., 2007. Estimation of vegetation parameter for modeling soil erosion using linear spectral mixture analysis of Landsat ETM data. ISPRS J. Photogramm. Remote Sens. 62, 309–324. http://dx.doi.org/10.1016/j.isprsjprs.2007.05.013.

de Asis, A.M., Omasa, K., Oki, K., Shimizu, Y., 2008. Accuracy and applicability of linear spectral unmixing in delineating potential erosion areas in tropical watersheds. Int. J. Remote Sens. 29, 4151–4171. http://dx.doi.org/10.1080/01431160701874579.

Bachmann, M., 2007. Automatisierte Ableitung von Bodenbedeckungsgraden durch MESMA-Entmischung. (Würzburg).

Ballabio, C., Borrelli, P., Spinoni, J., Meusburger, K., Michaelides, S., Beguería, S., Klik, A., Petan, S., Janeček, M., Olsen, P., Aalto, J., Lakatos, M., Rymszewicz, A., Dumitrescu, A., Tadić, M.P., Diodato, N., Kostalova, J., Rousseva, S., Banasik, K., Alewell, C., Panagos, P., 2017. Mapping monthly rainfall erosivity in Europe. Sci. Total Environ. 579, 1298–1315. http://dx.doi.org/10.1016/j.scitotenv.2016.11.123.

Bänninger, D., Brodbeck, M., Hohwieler, N., Meusburger, K., Alewell, C., 2006. Soil degradation in the Swiss Alps. In: Bierlin, B., Pasotti, J. (Eds.), Deserts and Desertification in High Altitude Areas, pp. 6–8.

Bätzing, W., 2015. Die Alpen. Geschichte und Zukunft einer europäischen Kulturlandschaft. München.

Biddoccu, M., Opsi, F., Cavallo, E., 2014. Relationship between runoff and soil losses with rainfall characteristics and long-term soil management practices in a hilly vineyard (piedmont, NW Italy). Soil Sci. Plant Nutr. 60, 92–99. http://dx.doi.org/10.1080/00380768.2013.862488.

Biddoccu, M., Ferraris, S., Opsi, F., Cavallo, E., 2016. Long-term monitoring of soil management effects on runoff and soil erosion in sloping vineyards in alto Monferrato (north–West Italy). Soil Tillage Res. 155, 176–189. http://dx.doi.org/10.1016/j.still.2015.07.005.

Bilotta, G.S., Brazier, R.E., Haygarth, P.M., 2007. The impacts of grazing animals on the quality of soils, vegetation, and surface waters in intensively managed grasslands. Adv. Agron. 94, 237–280. http://dx.doi.org/10.1016/S0065-2113(06)94006-1.

Blair, S., 2013. "V" for Vegetation. The mission of Proba-V. European Space Agency Bulletin 10–21.

Boardman, J.W., Kruse, F.A., 1994. Automated spectral analysis - a geological example using AVIRIS data, North Grapevine Mountains, Nevada. In: 10th Thematic Conference on Geologic Remote Sensing - Eploration, Environment, and Engineering, San Antonio, TX, pp. 407–418.

Bochet, E., Poesen, J., Rubio, J.L., 2006. Runoff and soil loss under individual plants of a semi-arid Mediterranean shrubland. Influence of plant morphology and rainfall intensity. Earth Surf. Process. Landf. 31, 536–549. http://dx.doi.org/10.1002/esp.1351.

Bosco, C., Rusco, E., Montanarella, L., Panagos, P., 2009. Soil erosion in the alpine area: risk assessment and climate change. Studi Trentini di Scienze Naturali 119–125.

Bötsch, M., 2004. Swiss agricultural policy and its focus on grassland. In: Lüscher, A., Jeangros, B., Kessler, W., Huguenin, O., Lobsiger, M., Millar, M., Suter, D. (Eds.), Land Use Systems in Grassland Dominated Regions, pp. 5–11 (Zürich).

Busetto, L., Colombo, R., Migliavacca, M., Cremonese, E., Meroni, M., Galvagno, M., Rossini, M., Siniscalco, C., Morra die Cella, U., Pari, E., 2010. Remote sensing of larch phenological cycle and analysis of relationships with climate in the Alpine region. Glob. Chang. Biol. 104, 88. http://dx.doi.org/10.1111/j.1365-2486.2010.02189.x.

Butt, M.J., Waqas, A., Mahmood, R., 2010. The combined effect of vegetation and soil erosion in the water resource management. Water Resour. Manag. 24, 3701–3714. http://dx.doi.org/10.1007/s11269-010-9627-7.

Camacho, F., 2016. Quality Assessment Report LAI, FAPAR, FCover Collection 300m. Version 1.

de Carvalho, D.F., Durigon, V.L., Antunes, M.A.H., Almeida, W.S.d., Oliveira, P.T.S.d, 2014. Predicting soil erosion using Rusle and NDVI time series from TM Landsat 5. Pesq. Agrop. Brasileira 49, 215–224. http://dx.doi.org/10.1590/S0100-204X2014000300008.

Ceaglio, E., Meusburger, K., Freppaz, M., Zanini, E., Alewell, C., 2012. Estimation of soil redistribution rates due to snow cover related processes in a mountainous area (Valle d'Aosta, NW Italy). Hydrol. Earth Syst. Sci. 16, 517–528. http://dx.doi.org/10.5194/hess-16-517-2012.

Chen, B., Huang, B., Xu, B., 2015. Comparison of spatiotemporal fusion models. A review. Remote Sens. 7, 1798–1835. http://dx.doi.org/10.3390/rs70201798.

Defila, C., Clot, B., 2001. Phytophenological trends in Switzerland. Int. J. Biometeorol. 45, 203–207. http://dx.doi.org/10.1007/s004840100101.

Dennison, P.E., Roberts, D.A., 2003. Endmember selection for multiple endmember spectral mixture analysis using endmember average RMSE. Remote Sens. Environ. 87, 123–135. http://dx.doi.org/10.1016/S0034-4257(03)00135-4.

Didan, K., Munoz, A.B., Solano, R., Huete, A., 2015. MOD13Q1 MODIS/Terra Vegetation Indices 16-Day L3 Global 250m SIN Grid V006. (Arizona).

Durán Zuazo, V.H., Rodríguez Pleguezuelo, C.R., 2008. Soil-erosion and runoff prevention by plant covers. A review. Agron. Sustain. Dev. 28, 65–86. http://dx.doi.org/10.1051/agro:2007062.

Efthimiou, N., 2016. Performance of the RUSLE in Mediterranean mountainous catchments. Environ. Processes 3, 1001–1019. http://dx.doi.org/10.1007/s40710-016-0174-y.

Ellenberg, H., Leuschner, C., Dierschke, H., 2010. Vegetation Mitteleuropas mit den Alpen. In ökologischer, dynamischer und historischer Sicht; 203 Tabellen, 6th ed. (Stuttgart).

Eshel, G., Egozi, R., Goldwasser, Y., Kashti, Y., Fine, P., Hayut, E., Kazukro, H., Rubin, B., Dar, Z., Keisar, O., DiSegni, D.M., 2015. Benefits of growing potatoes under cover crops in a Mediterranean climate. Agric. Ecosyst. Environ. 211, 1–9. http://dx.doi.org/10.1016/j.agee.2015.05.002.

Estrada-Carmona, N., Harper, E.B., DeClerck, F., Fremier, A.K., 2016. Quantifying model uncertainty to improve watershed-level ecosystem service quantification. A global sensitivity analysis of the RUSLE. Int. J. Biodiv. Sci. Ecosyst. Services Manag. 13, 40–50. http://dx.doi.org/10.1080/21513732.2016.1237383.

Federal Statistical Office Switzerland, 2017. Statistischer Atlas der Schweiz. 15.11.2017. https://www.atlas.bfs.admin.ch/maps/13/de/12714_5875_5874_4801/20931.html.

Felix, R., Johannes, B., 1995. Bodenerosionsuntersuchungen auf Testparzellen im Kalkhochgebirge. Mitteilungen der Österreichischen Geographischen Gesellschaft. 137. pp. 76–92.

Filippa, G., Cremonese, E., Galvagno, M., Migliavacca, M., Di Morra Cella, U., Petey, M., Siniscalco, C., 2015. Five years of phenological monitoring in a mountain grassland. Inter-annual patterns and evaluation of the sampling protocol. Int. J. Biometeorol. 59, 1927–1937. http://dx.doi.org/10.1007/s00484-015-0999-5.

Fontana, F., Rixen, C., Jonas, T., Aberegg, G., Wunderle, S., 2008. Alpine grassland phenology as seen in AVHRR, VEGETATION, and MODIS NDVI time series - a comparison with in situ measurements. Sensors 8, 2833–2853. http://dx.doi.org/10.3390/s8042833.

Foody, G.M., 2006. Sub-pixel methods in remote sensing. In: de Jong, S.M., van der Meer, F.D. (Eds.), Remote Sensing Image Analysis. Including the Spatial Domain. Dordrecht.

Frankenberg, P., Geier, B., Proswitz, E., Schutz, J., Seeling, S., 1995. Untersuchungen zu Bodenerosion und Massenbewegungen im Gunzesrieder Tal/Oberallgäu. Forstw. Cbl. 114, 214–231.

Frei, P., Kotlarski, S., Liniger, M.A., Schär, C., 2017. Snowfall in the Alps. Evaluation and projections based on the EURO-CORDEX regional climate models. Cryosphere Discuss. 1–38. http://dx.doi.org/10.5194/tc-2017-7.

Friedli, S., 2006. Digitale Bodenerosionsgefährdungskarte Der Schweiz Im Hektarraster – Unter Besonderer Berücksichtigung des Ackerlandes. (Bern).

Fuhrer, J., Beniston, M., Fischlin, A., Frei, C., Goyette, S., Jasper, K., Pfister, C., 2006. Climate risks and their impact on agriculture and forests in Switzerland. In: Wanner, H., Grosjean, M., Röthlisberger, R., Xoplaki, E. (Eds.), Climate Variability, Predictability and Climate Risks, pp. 79–102 (Dordrecht).

Gao, G.Y., Fu, B.J., Lü, Y.H., Liu, Y., Wang, S., Zhou, J., 2012. Coupling the modified SCS-

CN and RUSLE models to simulate hydrological effects of restoring vegetation in the Loess Plateau of China. Hydrol. Earth Syst. Sci. 16, 2347–2364. http://dx.doi.org/10.5194/hess-16-2347-2012.
García-Ruiz, J.M., Beguería, S., Nadal-Romero, E., González-Hidalgo, J.C., Lana-Renault, N., Sanjuán, Y., 2015. A meta-analysis of soil erosion rates across the world. Geomorphology 239, 160–173. http://dx.doi.org/10.1016/j.geomorph.2015.03.008.
Garonna, I., de Jong, R., de Wit, A.J.W., Mücher, C.A., Schmid, B., Schaepman, M.E., 2014. Strong contribution of autumn phenology to changes in satellite-derived growing season length estimates across Europe (1982-2011). Glob. Chang. Biol. 20, 3457–3470. http://dx.doi.org/10.1111/gcb.12625.
Gilabert, M., 2000. A mixture modeling approach to estimate vegetation parameters for heterogeneous canopies in remote sensing. Remote Sens. Environ. 72, 328–345. http://dx.doi.org/10.1016/S0034-4257(99)00109-1.
González, C., Resano, J., Mozos, D., Plaza, A., Valencia, D., 2010. FPGA implementation of the pixel purity index algorithm for remotely sensed hyperspectral image analysis. EURASIP J. Adv. Signal Process. 2010, 969806. http://dx.doi.org/10.1155/2010/969806.
Grauso, S., Verrubbi, V., Zini, A., Crovato, C., Sciortino, M., 2015. Soil Erosion Estimate in Southern Latium (Central Italy) Using RUSLE and Geostatistical Techniques. (Rome).
Grazhdani, S., Shumka, S., 2007. An approach to mapping soil erosion by water with application to Albania. Desalination 213, 263–272. http://dx.doi.org/10.1016/j.desal.2006.03.612.
Green, A.A., Berman, M., Switzer, P., Craig, M.D., 1988. A transformation for ordering multispectral data in terms of image quality with implications for noise removal. IEEE Trans. Geosci. Remote Sens. 26, 65–74. http://dx.doi.org/10.1109/36.3001.
Guerschman, J.P., Hill, M.J., Renzullo, L.J., Barrett, D.J., Marks, A.S., Botha, E.J., 2009. Estimating fractional cover of photosynthetic vegetation, non-photosynthetic vegetation and bare soil in the Australian tropical savanna region upscaling the EO-1 Hyperion and MODIS sensors. Remote Sens. Environ. 113, 928–945. http://dx.doi.org/10.1016/j.rse.2009.01.006.
Hawkins, R.H., 1985. Hydrology and the universal soil loss equation. Application to rangelands. In: US Department of the Interior, Technical Note. 365. pp. 1–40.
Heidari Mozaffar, M., Valadan Zoej, M.J., Sahebi, M.R., Rezaei, Y., 2008. Vegetation endmember extraction in Hyperion images. In: The International Archives of the Photogrammetry, Remote Sensing and Spatial Information Sciences. Vol. XXXVII. Part B7, Beijing, pp. 409–412.
Heinz, D.C., Chein-I-Chang, 2001. Fully constrained least squares linear spectral mixture analysis method for material quantification in hyperspectral imagery. IEEE Trans. Geosci. Remote Sens. 39, 529–545. http://dx.doi.org/10.1109/36.911111.
Hill, J., Mégier, J., Mehl, W., 1995. Land degradation, soil erosion and desertification monitoring in Mediterranean ecosystems. Remote Sens. Rev. 12, 107–130. http://dx.doi.org/10.1080/02757259509532278.
Hotz, M.-C., Weibel, F. (Eds.), 2005. Arealstatistik Schweiz. Zahlen, Fakten, Analysen. Neuchâtel.
Inoue, T., Nagai, S., Kobayashi, H., Koizumi, H., 2015. Utilization of ground-based digital photography for the evaluation of seasonal changes in the aboveground green biomass and foliage phenology in a grassland ecosystem. Eco. Inform. 25, 1–9. http://dx.doi.org/10.1016/j.ecoinf.2014.09.013.
Jeangros, B., Thomet, B., 2004. Multi-functionality of grassland systems in Switzerland. In: Lüscher, A., Jeangros, B., Kessler, W., Huguenin, O., Lobsiger, M., Millar, M., Suter, D. (Eds.), Land Use Systems in Grassland Dominated Regions, (Zürich).
Jonas, T., Rixen, C., Sturm, M., Stoeckli, V., 2008. How alpine plant growth is linked to snow cover and climate variability. J. Geophys. Res. 113, 377. http://dx.doi.org/10.1029/2007JG000680.
de Jong, S.M., 1994. Derivation of vegetation variables from a Landsat TM image for modelling soil erosion. Earth Surf. Process. Landf. 19. http://dx.doi.org/10.1002/esp.3290190207.
de Jong, S.M., Epema, G.F., 2010. Imaging spectrometry for surveying and modelling land degradation. In: van der Meer, F.D., de Jong, S.M. (Eds.), Imaging Spectrometry. Basic Principles and Prospective Applications. Dordrecht.
de Jong, S.M., Brouwer, L.C., Riezebos, H.T., 1998. Erosion Hazard Assessment in the La Peyne Catchment, France. Working Paper EU DeMon-II Project. Utrecht.
Jury, W.A., Horton, R., 2004. Soil Physics. Hoboken, NJ.
Karaburun, A., 2010. Estimation of C factor for soil erosion modeling using NDVI in Buyukcekmece watershed. Ozean J. Appl. Sci. 3, 77–85.
Karydas, C.G., Panagos, P., 2016. Modelling monthly soil losses and sediment yields in Cyprus. Int. J. Dig. Earth 9, 766–787. http://dx.doi.org/10.1080/17538947.2016.1156776.
Karydas, C.G., Panagos, P., 2017. The G2 erosion model. An algorithm for month-time step assessments. Environ. Res. 161, 256–267. http://dx.doi.org/10.1016/j.envres.2017.11.010.
Kerdiles, H., Grondona, M.O., 1995. NOAA-AVHRR NDVI decomposition and subpixel classification using linear mixing in the Argentinean pampa. Int. J. Remote Sens. 16, 1303–1325. http://dx.doi.org/10.1080/01431169508954478.
Keshava, N., Mustard, J.F., 2002. Spectral unmixing. IEEE Signal Process. Mag. 19, 44–57. http://dx.doi.org/10.1109/79.974727.
van der Knijff, J.M., Jones, R.J.A., Montanarella, L., 2000. Soil Erosion Risk Assessment in Italy. (Ispra).
Konz, N., Prasuhn, V., Alewell, C., 2012. On the measurement of alpine soil erosion. Catena 91, 63–71. http://dx.doi.org/10.1016/j.catena.2011.09.010.
Kulikov, M., Schickhoff, U., Borchardt, P., 2016. Spatial and seasonal dynamics of soil loss ratio in mountain rangelands of south-western Kyrgyzstan. J. Mt. Sci. 13, 316–329. http://dx.doi.org/10.1007/s11629-014-3393-6.
Lee, J.S., Won, J.Y., 2012. Suggestion of cover-management factor equation for mountain area in RUSLE. J.Korean Soc.Hazard Mitigation 12, 79–85.
Leilei, L., Jianrong, F., Yang, C., 2014. The relationship analysis of vegetation cover, rainfall and land surface temperature based on remote sensing in Tibet, China. IOP Conf. Ser. Earth and Environ. Sci. 17, 12034. http://dx.doi.org/10.1088/1755-1315/17/1/012034.
López-Vicente, M., Navas, A., Machín, J., 2008. Identifying erosive periods by using RUSLE factors in mountain fields of the Central Spanish Pyrenees. Hydrol. Earth Syst. Sci. 12, 523–535. http://dx.doi.org/10.5194/hess-12-523-2008.
Lu, D., Li, G., Valladares, G.S., Batistella, M., 2004. Mapping soil erosion risk in Rondônia, Brazilian Amazonia. Using RUSLE, remote sensing and GIS. Land Degrad. Dev. 15, 499–512. http://dx.doi.org/10.1002/ldr.634.
Lugato, E., Panagos, P., Bampa, F., Jones, A., Montanarella, L., 2014. A new baseline of organic carbon stock in European agricultural soils using a modelling approach. Glob. Chang. Biol. 20, 313–326. http://dx.doi.org/10.1111/gcb.12292.
Ma, J.W., Xue, Y., Ma, C.F., Wang, Z.G., 2003. A data fusion approach for soil erosion monitoring in the upper Yangtze River basin of China based on universal soil loss equation (USLE) model. Int. J. Remote Sens. 24, 4777–4789. http://dx.doi.org/10.1080/0143116021000056028.
Maetens, W., Vanmaercke, M., Poesen, J., Jankauskas, B., Jankauskiene, G., Ionita, I., 2012. Effects of land use on annual runoff and soil loss in Europe and the Mediterranean. Prog. Phys. Geogr. 36, 599–653. http://dx.doi.org/10.1177/0309133312451303.
Mancino, G., Nolè, A., Salvati, L., Ferrara, A., 2016. In-between forest expansion and cropland decline. A revised USLE model for soil erosion risk under land-use change in a Mediterranean region. Ecol. Indic. 71, 544–550. http://dx.doi.org/10.1016/j.ecolind.2016.07.040.
Martin, C., Pohl, M., Alewell, C., Körner, C., Rixen, C., 2010. Interrill erosion at disturbed alpine sites. Effects of plant functional diversity and vegetation cover. Basic Appl. Ecol. 11, 619–626. http://dx.doi.org/10.1016/j.baae.2010.04.006.
Mather, P.M., Koch, M., 2011. Computer Processing of Remotely-Sensed Images. An Introduction. (4th Ed.). Hoboken, N.J., Chichester.
Mayer, R., Kaufmann, R., Vorhauser, K., Erschbamer, B., 2009. Effects of grazing exclusion on species composition in high-altitude grasslands of the central alps. Basic Appl. Ecol. 10, 447–455. http://dx.doi.org/10.1016/j.baae.2008.10.004.
McCool, D.K., Foster, G.R., Renard, K.G., Yoder, D.C., Weesies, G.A., 1995. The Revised Universal Soil Loss Equation. Interagency Workshop on Technologies to Address Soil Erosion on Department of Defense Lands, San Antonio, TX.
van der Meer, F.D., 2002. Image classification through spectral unmixing. In: Stein, A., van der Meer, F.D., Gorte, B. (Eds.), Spatial Statistics for Remote Sensing. Dordrecht.
van der Meer, F.D., 2010. Basic physics of spectrometry. In: van der Meer, F.D., de Jong, S.M. (Eds.), Imaging Spectrometry. Basic Principles and Prospective applications. Dordrecht.
van der Meer, F.D., de Jong, S.M., 2000. Improving the results of spectral unmixing of Landsat thematic mapper imagery by enhancing the orthogonality of end-members. Int. J. Remote Sens. 21, 2781–2797. http://dx.doi.org/10.1080/01431160050121249.
Merz, A., Alewell, C., Hiltbrunner, E., Banninger, D., 2009. Plant-compositional effects on surface runoff and sediment yield in subalpine grassland. J. Plant Nutr. Soil Sci. 172, 777–788. http://dx.doi.org/10.1002/jpln.200800231.
Meusburger, K., Alewell, C. (Eds.), 2014. Soil Erosion in the alps. Experience gained from case studies (2006–2013). Bernoulli.
Meusburger, K., Bänninger, D., Alewell, C., 2010a. Estimating vegetation parameter for soil erosion assessment in an alpine catchment by means of QuickBird imagery. Int. J. Appl. Earth Obs. Geoinf. 12, 201–207. http://dx.doi.org/10.1016/j.jag.2010.02.009.
Meusburger, K., Konz, N., Schaub, M., Alewell, C., 2010b. Soil erosion modelled with USLE and PESERA using QuickBird derived vegetation parameters in an alpine catchment. Int. J. Appl. Earth Obs. Geoinf. 12, 208–215. http://dx.doi.org/10.1016/j.jag.2010.02.004.
Meusburger, K., Steel, A., Panagos, P., Montanarella, L., Alewell, C., 2012. Spatial and temporal variability of rainfall erosivity factor for Switzerland. Hydrol. Earth Syst. Sci. 16, 167–177. http://dx.doi.org/10.5194/hess-16-167-2012.
Meusburger, K., Leitinger, G., Mabit, L., Mueller, M.H., Walter, A., Alewell, C., 2014. Soil erosion by snow gliding – a first quantification attempt in a subalpine area in Switzerland. Hydrol. Earth Syst. Sci. 18, 3763–3775. http://dx.doi.org/10.5194/hess-18-3763-2014.
Möller, M., Gerstmann, H., Gao, F., Dahms, T.C., Förster, M., 2017. Coupling of phenological information and simulated vegetation index time series. Limitations and potentials for the assessment and monitoring of soil erosion risk. Catena 150, 192–205. http://dx.doi.org/10.1016/j.catena.2016.11.016.
Montandon, L.M., Small, E.E., 2008. The impact of soil reflectance on the quantification of the green vegetation fraction from NDVI. Remote Sens. Environ. 112, 1835–1845. http://dx.doi.org/10.1016/j.rse.2007.09.007.
Nascimento, J.M.P., Dias, J.M.B., 2005. Vertex component analysis. A fast algorithm to unmix hyperspectral data. IEEE Trans. Geosci. Remote Sens. 43, 898–910. http://dx.doi.org/10.1109/TGRS.2005.844293.
Nearing, M.A., Jetten, V., Baffaut, C., Cerdan, O., Couturier, A., Hernandez, M., Le Bissonnais, Y., Nichols, M.H., Nunes, J.P., Renschler, C.S., Souchère, V., van Oost, K., 2005. Modeling response of soil erosion and runoff to changes in precipitation and cover. Catena 61, 131–154. http://dx.doi.org/10.1016/j.catena.2005.03.007.
Ozcan, A.U., Erpul, G., Basaran, M., Erdogan, H.E., 2008. Use of USLE/GIS technology integrated with geostatistics to assess soil erosion risk in different land uses of Indagi Mountain Pass—Çankırı, Turkey. Environ. Geol. 53, 1731–1741. http://dx.doi.org/10.1007/s00254-007-0779-6.
Pal, S.K., Majumdar, T.J., Bhattacharya, A.K., Bhattacharyya, R., 2011. Utilization of Landsat ETM+ data for mineral-occurrences mapping over Dalma and Dhanjori, Jharkhand, India. An advanced spectral analysis approach. Int. J. Remote Sens. 32, 4023–4040. http://dx.doi.org/10.1080/01431161.2010.484430.
Panagos, P., Karydas, C.G., Gitas, I.Z., Montanarella, L., 2012. Monthly soil erosion

monitoring based on remotely sensed biophysical parameters. A case study in Strymonas river basin towards a functional pan-European service. Int. J. Digital Earth 5, 461–487. http://dx.doi.org/10.1080/17538947.2011.587897.
Panagos, P., Karydas, C., Borrelli, P., Ballabio, C., Meusburger, K., 2014a. Advances in Soil Erosion Modelling through Remote Sensing Data Availability at European Scale. In: Second International Conference on Remote Sensing and Geoinformation of the Environment 12th August 2014, pp. 92290I. http://dx.doi.org/10.1117/12.2066383.
Panagos, P., Christos, K., Cristiano, B., Ioannis, G., 2014b. Seasonal monitoring of soil erosion at regional scale. An application of the G2 model in Crete focusing on agricultural land uses. Int. J. Appl. Earth Obs. Geoinf. 27, 147–155. http://dx.doi.org/10.1016/j.jag.2013.09.012.
Panagos, P., Borrelli, P., Poesen, J., Ballabio, C., Lugato, E., Meusburger, K., Montanarella, L., Alewell, C., 2015a. The new assessment of soil loss by water erosion in Europe. Environ. Sci. Pol. 54, 438–447. http://dx.doi.org/10.1016/j.envsci.2015.08.012.
Panagos, P., Borrelli, P., Meusburger, K., Alewell, C., Lugato, E., Montanarella, L., 2015b. Estimating the soil erosion cover-management factor at the European scale. Land Use Policy 48, 38–50. http://dx.doi.org/10.1016/j.landusepol.2015.05.021.
Panagos, P., Borrelli, P., Meusburger, K., van der Zanden, E.H., Poesen, J., Alewell, C., 2015c. Modelling the effect of support practices (P-factor) on the reduction of soil erosion by water at European scale. Environ. Sci. Pol. 51, 23–34. http://dx.doi.org/10.1016/j.envsci.2015.03.012.
Panagos, P., Borrelli, P., Spinoni, J., Ballabio, C., Meusburger, K., Beguería, S., Klik, A., Michaelides, S., Petan, S., Hrabalíková, M., Olsen, P., Aalto, J., Lakatos, M., Rymszewicz, A., Dumitrescu, A., Perčec Tadić, M., Diodato, N., Kostalova, J., Rousseva, S., Banasik, K., Alewell, C., 2016. Monthly rainfall erosivity. conversion factors for different time resolutions and regional assessments. WaterSA 8, 119. http://dx.doi.org/10.3390/w8040119.
Paringit, E.C., Nadaoka, K., 2003. Sediment yield modelling for small agricultural catchments. Land-cover parameterization based on remote sensing data analysis. Hydrol. Process. 17, 1845–1866. http://dx.doi.org/10.1002/hyp.1222.
Phillips, D.L., Newsome, S.D., Gregg, J.W., 2005. Combining sources in stable isotope mixing models. Alternative methods. Oecologia 144, 520–527. http://dx.doi.org/10.1007/s00442-004-1816-8.
Pohl, M., Alig, D., Körner, C., Rixen, C., 2009. Higher plant diversity enhances soil stability in disturbed alpine ecosystems. Plant Soil 324, 91–102. http://dx.doi.org/10.1007/s11104-009-9906-3.
Puigdefábregas, J., 2005. The role of vegetation patterns in structuring runoff and sediment fluxes in drylands. Earth Surf. Process. Landf. 30, 133–147. http://dx.doi.org/10.1002/esp.1181.
Rajczak, J., Schär, C., 2017. Projections of future precipitation extremes over Europe. A multimodel assessment of climate simulations. J. Geophys. Res. Atmos. 122, 10773–10800. http://dx.doi.org/10.1002/2017JD027176.
Rajczak, J., Pall, P., Schär, C., 2013. Projections of extreme precipitation events in regional climate simulations for Europe and the alpine region. J. Geophys. Res. Atmos. 118, 3610–3626. http://dx.doi.org/10.1002/jgrd.50297.
Rammig, A., Jonas, T., Zimmermann, N.E., Rixen, C., 2010. Changes in alpine plant growth under future climate conditions. Biogeosciences 7, 2013–2024. http://dx.doi.org/10.5194/bg-7-2013-2010.
Renard, K.G., Freimund, J.R., 1994. Using monthly precipitation data to estimate the R-factor in the revised USLE. J. Hydrol. 157, 287–306. http://dx.doi.org/10.1016/0022-1694(94)90110-4.
Renard, K.G., Foster, G., Weesies, G., McCool, D.K., Yoder, D.C., 1997. Prediction Soil Erosion by Water: A Guide to Conservation Planning with the Revised Universal Soil Loss Equation (RUSLE). USDA Agriculture Handbook. 703.
Roberts, D.A., Smith, M.O., Adams, J.B., 1993. Green vegetation, nonphotosynthetic vegetation, and soils in AVIRIS data. Remote Sens. Environ. 44, 255–269. http://dx.doi.org/10.1016/0034-4257(93)90020-X.
Roberts, D.A., Batista, G.T., Pereira, J., Waller, E.K., Nelson, B.W., 1999. Change identification using multitemporal spectral mixture analysis: applications in Eastern Amazonia. In: Elvidge, C.D., Lunetta, R.S. (Eds.), Remote Sensing Change Detection. Environmental Monitoring Methods and Applications, pp. 137–161 (Chelsea, Mich).
Rogge, D.M., Rivard, B., Zhang, J., Sanchez, A., Harris, J., Feng, J., 2007. Integration of spatial–spectral information for the improved extraction of endmembers. Remote Sens. Environ. 110, 287–303. http://dx.doi.org/10.1016/j.rse.2007.02.019.
RSI Research Systems, I, 2004. ENVI User's Guide.
Schindler Wildhaber, Y., Bänninger, D., Burri, K., Alewell, C., 2012. Evaluation and application of a portable rainfall simulator on subalpine grassland. Catena 91, 56–62. http://dx.doi.org/10.1016/j.catena.2011.03.004.
Schmidli, J., Frei, C., 2005. Trends of heavy precipitation and wet and dry spells in Switzerland during the 20th century. Int. J. Climatol. 25, 753–771. http://dx.doi.org/10.1002/joc.1179.
Schmidli, J., Schmutz, C., Frei, C., Wanner, H., Schär, C., 2002. Mesoscale precipitation variability in the region of the European alps during the 20th century. Int. J. Climatol. 22, 1049–1074. http://dx.doi.org/10.1002/joc.769.
Schmidt, S., Alewell, C., Panagos, P., Meusburger, K., 2016. Regionalization of monthly rainfall erosivity patterns in Switzerland. Hydrol. Earth Syst. Sci. 20, 4359–4373. http://dx.doi.org/10.5194/hess-20-4359-2016.
Schmidt, S., Alewell, C., Meusburger, K., 2018. Swiss National Grassland Map and Change (1996–2015) of Permanent Grasslands Extent in Switzerland. Data in Brief, submitted.
Schwertmann, U., Vogl, W., Kainz, M., 1987. Bodenerosion durch Wasser. Vorhersage des Abtrags und Bewertung von Gegenmaßnahmen. Stuttgart.
Smets, B., Jacobs, T., Verger, A., 2017. Product User Manual. Leaf Area Index (LAI), Fraction of Photosynthetically Active Radiation (FAPAR), Fraction of Vegetation Cover (FCover), Collection 300m, Version 1. VITO.
Smith, M.O., Johnson, P.E., Adams, J.B., 1985. Quantitative determination of mineral types and abundances from reflectance spectra using principal components analysis. J. Geophys. Res. 90, C797. http://dx.doi.org/10.1029/JB090iS02p0C797.
Smith, M.O., Ustin, S.L., Adams, J.B., Gillespie, A.R., 1990. Vegetation in desertsI. A regional measure of abundance from multispectral images. Remote Sens. Environ. 31, 1–26. http://dx.doi.org/10.1016/0034-4257(90)90074-V.
Stanchi, S., Freppaz, M., Ceaglio, E., Maggioni, M., Meusburger, K., Alewell, C., Zanini, E., 2014. Soil erosion in an avalanche release site (Valle d'Aosta. Italy): towards a winter factor for RUSLE in the alps. Nat. Hazards Earth Syst. Sci. 14, 1761–1771. http://dx.doi.org/10.5194/nhess-14-1761-2014.
Studer, S., Appenzeller, C., Defila, C., 2005. Inter-annual variability and decadal trends in alpine spring phenology. A multivariate analysis approach. Clim. Chang. 73, 395–414. http://dx.doi.org/10.1007/s10584-005-6886-z.
Sun, W., Shao, Q., Liu, J., 2013. Soil erosion and its response to the changes of precipitation and vegetation cover on the loess plateau. J. Geogr. Sci. 23, 1091–1106. http://dx.doi.org/10.1007/s11442-013-1065-z.
Sutter, R., 2007. Erosion im Alpgebiet. Schlussbericht. Appenzell.
Sutter, R., Keller, L., 2009. Bodenerosion im Sömmerungsgebiet. Erkennen - vermeiden - beheben. Lindau.
Swisstopo, 2010. SWISSIMAGE. Das digitale Farborthophotomosaik der Schweiz. Wabern.
Swisstopo, 2017a. swissALTI3D. Das hochaufgelöste Terrainmodell der Schweiz. Wabern.
Swisstopo, 2017b. Swissimage RS. 21.12.2017. https://shop.swisstopo.admin.ch/de/products/images/ortho_images/SWISSIMAGE_RS.
Theseira, M.A., Thomas, G., Taylor, J.C., Gemmell, F., Varjo, J., 2003. Sensitivity of mixture modelling to end-member selection. Int. J. Remote Sens. 24, 1559–1575. http://dx.doi.org/10.1080/01431160210146631.
Troxler, J., Chatelain, C., Schwery, M., 2004. Technical and economical evaluation of grazing systems for high altitude sheep pastures in Switzerland. In: Lüscher, A., Jeangros, B., Kessler, W., Huguenin, O., Lobsiger, M., Millar, M., Suter, D. (Eds.), Land Use Systems in Grassland Dominated Regions, pp. 590–592 (Zürich).
Vatandaşlar, C., Yavuz, M., 2017. Modeling cover management factor of RUSLE using very high-resolution satellite imagery in a semiarid watershed. Environ. Earth Sci. 76, 267. http://dx.doi.org/10.1007/s12665-017-6388-0.
Vrieling, A., 2006. Satellite remote sensing for water erosion assessment. A review. Catena 65, 2–18. http://dx.doi.org/10.1016/j.catena.2005.10.005.
Vrieling, A., de Jong, S.M., Sterk, G., Rodrigues, S.C., 2008. Timing of erosion and satellite data. A multi-resolution approach to soil erosion risk mapping. Int. J. Appl. Earth Obs. Geoinf. 10, 267–281. http://dx.doi.org/10.1016/j.jag.2007.10.009.
Vrieling, A., Hoedjes, J.C.B., van der Velde, M., 2014. Towards large-scale monitoring of soil erosion in Africa. Accounting for the dynamics of rainfall erosivity. Glob. Planet. Chang. 115, 33–43. http://dx.doi.org/10.1016/j.gloplacha.2014.01.009.
Wang, G., Wente, S., Gertner, G.Z., Anderson, A., 2002. Improvement in mapping vegetation cover factor for the universal soil loss equation by geostatistical methods with Landsat thematic mapper images. Int. J. Remote Sens. 23, 3649–3667. http://dx.doi.org/10.1080/01431160110114538.
Wang, B., Yang, Q., Liu, Z., 2009. Effect of conversion of farmland to forest or grassland on soil erosion intensity changes in Yanhe River basin, loess plateau of China. Front. Forest. China 4, 68–74. http://dx.doi.org/10.1007/s11461-009-0015-5.
Weiss, M., Baret, F., Myneni, R.B., Pragnère, A., Knyazikhin, Y., 2000. Investigation of a model inversion technique to estimate canopy biophysical variables from spectral and directional reflectance data. Agronomie 20, 3–22. http://dx.doi.org/10.1051/agro:2000105.
Widmann, M., Schär, C., 1997. A principal component and long-term trend analysis of daily precipitation in Switzerland. Int. J. Climatol. 17, 1333–1356. http://dx.doi.org/10.1002/(SICI)1097-0088(199710)17:12<1333::AID-JOC108>3.0.CO;2-Q.
Wiegand, T., Wiegand, K., Pütz, S., 2008. Grassland models. In: Encyclopedia of Ecology, pp. 1754–1765 (Amsterdam).
Wischmeier, W.H., Smith, D.D., 1965. Predicting Rainfall-Erosion Losses from Cropland East of the Rocky Mountains. (Washington).
Wischmeier, W.H., Smith, D.D., 1978. Predicting Rainfall Erosion Losses. (Washington).
Yang, X., 2014. Deriving RUSLE cover factor from time-series fractional vegetation cover for hillslope erosion modelling in new South Wales. Soil Res. 52, 253. http://dx.doi.org/10.1071/SR13297.
Yong-Zhong, S., Yu-Lin, L., Jian-Yuan, C., Wen-Zhi, Z., 2005. Influences of continuous grazing and livestock exclusion on soil properties in a degraded sandy grassland, Inner Mongolia, northern China. Catena 59, 267–278. http://dx.doi.org/10.1016/j.catena.2004.09.001.
Zhang, W., Li, H., 2015. RUSLE and GIS-based assessment of soil erosion in the mountain areas of Beijing, China. In: International Conference on Advances in Energy and Environment Science ICAEES.
Zhang, Y., Liu, B.-Y., Zhang, Q.-C., Xie, Y., 2003. Effect of different vegetation types on soil erosion by water. Acta Bot. Sin. 45, 1204–1209.
Zhang, W., Zhang, Z., Liu, F., Qiao, F., Hu, S., 2011. Estimation of the USLE cover and management factor C using setellite remote sensing: A review. 19th International Conference on Geoinformatics 24.06.2011–26.06.2011, Shanghai.Estimation of the USLE cover and management factor C using setellite remote sensing: A review. 19th International Conference on Geoinformatics 24.06.2011–26.06.2011, Shanghai.
Zhou, P., Luukkanen, O., Tokola, T., Nieminen, J., 2008. Effect of vegetation cover on soil erosion in a mountainous watershed. Catena 75, 319–325. http://dx.doi.org/10.1016/j.catena.2008.07.010.
Zwingli, H., 2017. Statistik zur Heumahd. Email. St. Gallen.